Characterizing Behaviors and Functions of Joints for Design of Origami-Based Mechanical Systems

Nathan Chandler Brown

A thesis submitted to the faculty of
Brigham Young University
in partial fulfillment of the requirements for the degree of

Master of Science

Spencer P. Magleby, Chair
Larry L. Howell
Steven K. Charles

Department of Mechanical Engineering

Brigham Young University

ABSTRACT

Characterizing Behaviors and Functions of Joints for Design of
Origami-Based Mechanical Systems

Nathan Chandler Brown
Department of Mechanical Engineering, BYU
Master of Science

This thesis addresses a number of challenges designers face when designing deployable origami-based arrays, specifically joint selection, design, and placement within an array. In deployable systems, the selection and arrangement of joint types is key to how the system functions. The kinematics and performance of an array is directly affected by joint performance. This work develops joint metrics which are then used to compare joint performances, constructing a tool designers can use when selecting joints for an origami array. While often a single type of joint is used throughout an array, this work shows how using multiple types of joints within the same array can offer benefits for motion deployment, and array stiffening.

Origami arrays are often used for their unique solutions for stowing and deploying large planar shapes. Folds, enabled through joints, within these patterns allow the arrays to fold compactly. However, it can be difficult to fully deploy arrays, particularly array designs with a high number of joints. In addition, it is a challenge to stabilize a fully deployed array from undesired re-folding. This work introduces a strain-energy storing joint that is used to deploy and stiffen foldable origami arrays, the Lenticular Lock (LentLock). Geometry of the LentLock is introduced and the deploying and stiffening performance of the joint is shown.

Folds within an origami array create the constraints that link motion between panels, and can be used to create kinematic benefits, such as creating mechanisms with a single degree-of-freedom. While many fold-constraints are required to define motion, this work shows that origami-based system contain many redundant constraints. The removal of redundant joints does not affect the motion of the array nor the observed mobility, but may decrease the likelihood of binding, simplify the overall system and decrease actuation force. This work introduces a visual and iterative approach designers can use to identify redundant constraints in origami patterns, and techniques that can be used to remove the identified redundant constraints. The presented techniques are demonstrated by removing redundant constraints from prototyped origami mechanisms.

As a result of this work, designers will be better able to approach and design deployable origami-based mechanisms.

Keywords: origami-based design, deployable, overconstrained mechanisms, mobile overconstrained mechanisms, joint, strain energy, compliant mechanisms

ACKNOWLEDGMENTS

I would like to thank everyone in the Compliant Mechanisms Research Group at Brigham Young University, acknowledging specific colleagues Collin Ynchausti, Brandon Sargent, Jared Butler, Hunter Pruett, Dan Ames, and Diana Bolaños, whose open and collaborative nature enabled a safeguarded place for brainstorming, collaboration and learning. I am grateful for my collaborators Terri Bateman, Robert J. Lang, and those at Florida International University, including Abdul Sattar-Kaddour, Antonio Jose Rubio, and Stavros V. Georgakopoulos.

I would like to acknowledge my funding through the Air Force Office of Scientific Research under Grant No. FA9550-19-1-0290 through Florida International University, and Durrant and Associates, which enabled my work.

I would like to thank graduate committee member Dr. Steven Charles, whose exemplary example of teaching, both formally and informally, motivates me push the limits of my knowledge and enliven the spirit of learning in others.

My co-advisor Dr. Howell, who rather than merely overseeing my research and career path, took every opportunity to build me up, and impart his experience as an admirable researcher, professor and professional. His shared analogies, stories, and experiences have reshaped my perception of what it means to be an advisor.

I would like to extend a special thank you to my graduate advisor and committee chair Dr. Spencer Magleby. His vision and excitement about design is contagious and has encouraged me to savor creativity. Dr. Magleby's positive and confident nature invigorated my research with a sense of purpose, and reminded me to stop and consider the progress that has been made.

I want to express gratitude for divine inspiration and guidance, which had an integral part in my work and resolve to succeed. Lastly, I would like to thank my wife, Ali, and my kids, Luke and Mikelle. Ali's support and far seeing perspective fortified my motivation and encouraged me to enjoy the journey.

TABLE OF CONTENTS

LIST OF TABLES

LIST OF FIGURES

NOMENCLATURE

ϕ	Angle of twist
G	Shear Modulus
L_{flex}	Flexure length
b	Flexure thickness
h_{flex}	Flexure width
β	Material property dependant on ratio b/h_{flex}
k_t	Torsional stiffness
L_{unit}	Length of each waistband unit
L_{con}	Waistband connecting element length
E	Young's Modulus
δ	Flexure deflection
k_b	Flexure Bending stiffness
F_b	Bending force of a rectangular beam
T	Torque of rectangular beam in torsion
c_u	Undeflected waistband circumference
c_d	Deflected waistband circumference
δ_{total}	Combined flexure deflection
n_{units}	Number of waistband units
M	Mobility
α	Sector angles
γ	Fold angles
λ	Constraint Space
N	Number of links
J	Number of joints
f_i	Degrees of freedom permitted by joint i
n	Vertex degree
B	Number of edges on the border of the pattern
H	Number of holes within an origami pattern
S	Number of redundant constraints
P_k	Number of k-gon facets in an origami pattern
j	Number of joints
V	Number of internal vertices
W	Panel width
s	Arc length along a curve
L	Total arc length
κ_0	Initial curvature
$x(s)$	Position in X direction
$y(s)$	Position in Y direction
F_{Latch}	Latching force
L	Curve length
t_f	Flexure thickness
t_p	Panel thickness
F_f	Flexure force

n_m	Total system degrees of freedom
P	Number of parallel LET joints in an array
S	Number of LET joints of an array in series
k_{eq}	Equivalent stiffness
M_x	Moment in X direction
M_y	Moment in Y direction
σ_{max}	Maximum stress
σ_T	Tensile strength

CHAPTER 1. INTRODUCTION

Origami, the ancient art of paper folding, has introduced new approaches to mechanism design. Mathematicians and engineers have recently developed methods to incorporate principles of origami art into real-world engineering applications. Origami-based design has become a branch of compliant mechanism research, inspiring an alternative solution to traditional design methods that reduces cost [2] by replacing traditional hinges, joints, or other moving parts with flexible members.

Origami has inspired designs for minimally invasive surgical equipment [3, 4], bellows for extraterrestrial drilling [5], magnetically controlled bistable microrobots [6], expanding heart stents [7], and structural composites [8].

Principles of origami offer unique solutions for deployable structures used in aerospace design. While solar panels and communication hardware can be attached to the sides of spacecraft, the maximum aperture area for these designs is limited to the surface area of the spacecraft exterior. Foldable and deployable origami arrays allow larger array apertures to be stored compactly during spacecraft launch and then deploy once in orbit. This ability allows larger arrays to be used, resulting in increased power generation and higher antenna gains. Deployable designs have included a deployable flasher-patterned solar array [9, 10], a self-stiffening and retractable deployable space array [11], foldable antennas [12–16] and deployable solar panels [17–19].

For these foldable designs to function, rigid panels must be joined by a region with lower stiffness to allow hinge-like rotation between relative panels. Traditional mechanisms use pins or hinges to provide the motion, however many joint types have been developed and analyzed [9,20–23].

While these joints enable the folding motion of the overall array, they can become a challenge in multiple ways. If joints are not aligned properly within an array, the overall mechanism will bind. Joints that are not properly stabilized once in the deployed state can cause the array to re-fold. In addition, while compliant joints can offer deployment motions that are useful, they also can suffer from parasitic motions, meaning that loads can cause movement between panels in undesired directions.

This thesis explores the design of deployable mechanisms, focusing on joint design and placement within deployable origami arrays. The objective of this thesis is to develop techniques designers can use when designing deployable systems, with special focus on joint function and utilization. Chapter 2[1] discusses a circular deployable system where stiffnesses to parasitic motions were utilized. Chapter 3[2] analyzes the constraints of single-degree-of-freedom (1-DoF) deployable systems and presents several techniques to reduce overconstraint. Chapter 4[3] presents a compliant hinge design used to deploy and stiffen origami arrays at its joints, and will be submitted as a paper. Chapter 5 includes thoughts collected during research on joint characterization and selection for improved mechanism performance. Chapter 6[4] presents three case-studies where deployable mechanisms were designed to ensure predictable deployment for reconfigurable reflectarray antennas.

1.1 Background

To better understand the research presented below, three concepts will be briefly reviewed. Thickness accommodation techniques for thick origami will be summarized. Current joints used to enable relative motion between rigid origami panels will also be noted. Since many of these principles will be applied to deployable spacecraft antennas, a short description of CubeSat antenna technologies will also be given.

1.1.1 Thickness Accommodation Techniques

Origami has enabled new approaches to designing solutions to engineering problems, such as deployable arrays. Paper and folding patterns can be used to synthesize foldable arrays with certain characteristics such as a single degree of freedom. However, as we move from designing in

[1] Chapter based on publication [24]
[2] Chapter based on publication [25]
[3] To be submitted for publication
[4] Chapter based on publications [26–28]

paper to using engineering materials with non-negligible thicknesses, considerations must be made as to how to accommodate for the material thickness. Accommodation techniques take into account the thickness of the material and allow folding motion through specific placement of hinges and offset links.

Many thickness accommodation techniques have been developed. While membranes can be used as a hinge between rigid panels, it has been shown that membranes can also be used to accommodate thickness [9]. In the tapered panels technique, panels are volumetrically trimmed along the bisection of the dihedral angles of each joint to allow the pattern to partly fold [29]. Edmondson et al. proposed the offset panel technique that utilizes offsets to position the panels away from the zero thickness model, allowing the panels to stack parallel to one another [30, 31]. With the hinge shift technique, rotational axes are shifted to the edge of the material, often alternating sides. The doubled hinged technique, sometimes implemented as the offset crease technique [32], splits a single fold into two, expanding the crease area to a size that accommodates the material thickness. Rolling contact techniques such as the compliant rolling-contact element (CORE) joint [21, 22] and synchronized offset rolling contact element (SORCE) joints [33] can also be used in thick-folding mechanisms. Pehrson et al. developed the strained joint technique by implementing surrogate folds as a means to allow for the panels to fold while simultaneously creating the needed panel offset [34].

Lang et al. provided a review of many current accommodation techniques, discussing their kinematic properties, and ease of implementation into folding patterns [35]. In the same review, it is discussed how multiple techniques can be combined into the same vertex or into the larger folding pattern. This review gives the designer a "tool" to compare thickness accommodation techniques and choose one that best fits their design.

1.1.2 Current Joint Types

The folding motion in any foldable array is made possible through its joints. A joint is a part of the array around which adjacent the panels can rotationally articulate. Because various hinges have different performances, a designer may choose to use any type of joint. Joints such as a traditional pin-joint hinge are often used because of they are simple to apply and involve very little extra design work. However, there are many joint types that offer benefits to certain design circumstances.

Some of these joint types include: the standard hinge, Lamina Emergent Torsional (LET) joint [20], variations of the LET joint [36–41], membrane hinge [9], CORE joint [21, 22], ReCS technique joint [23], and many more [33, 42, 43].

Each joint type offers benefits and drawbacks which are defined by the desired joint behavior. In other words, the desired behavior defines whether a certain aspect of a joint's behavior is beneficial or poor. For example, a LET joint is useful because it stores strain energy that could be used in an array for self-deployment. The LET joint also enables a very large range of motion. However, this joint is very liable to parasitic motions, or undesired motions, and generally cause adverse effects in a design. On the other hand, whether or not a motion is desired or parasitic depends on the application. For example, work published by Pehrson et al. showed that motions that are generally thought of as parasitic actually made the pattern's motion possible [11]. In this case, the off-axis motion is desirable.

1.1.3 CubeSat Reflectarrays

A CubeSat is a small satellite used for space research that is made up of one or multiple cube-shaped units. CubeSat missions for low-earth orbit have become widely accepted and utilized to enable new opportunities for space exploration. Two main advantages CubeSats have over other spacecraft technologies is a short design time and low fabrication cost as components are generally purchased pre-made from component suppliers.

CubeSats often use high gain antennas (HGAs) for communication as they can transmit signals longer distances while requiring a low amount of power. HGAs such as parabolic reflectors are generally heavy, bulky and have a large surface area. To alleviate these problems, microstrip patch reflectarrays (RA) can be used to replace the parabolic reflectors. RAs are a type of antenna that is made from PCB material, with patches of copper material etched into the material in an array pattern. The patches are designed such that the planar reflectarray antenna exhibits similar behavior to that of a parabolic antenna. The planar nature of these RAs enable more efficient ways of folding, stowing, and deploying the RA.

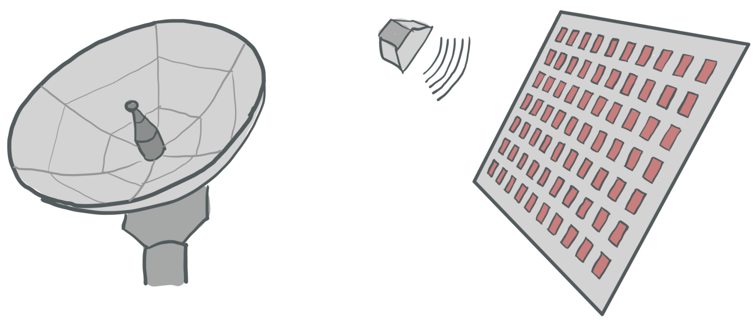

Figure 1.1: Two types of high gain antennas. A parabolic antenna (left) has a doubly-curved shape that is used to reflect electromagnetic waves to and from the feed/receiver. A microstrip patch reflectarray (right), which includes a flat geometry.

CHAPTER 2. ORIGAMI-INSPIRED DEPLOYABLE WAISTBAND SYSTEM THAT IMPROVES ADULT DIAPER PERFORMANCE

2.1 Motivation

Diapers have been traditionally used to alleviate the effects of incontinence in users from all demographics. Many companies and medical researchers have worked to create new technologies to improve adult diapers to better suit the needs of their users. Current diaper solutions include absorbent liners, perineal pads, reusable absorbent underwear, and disposable adult diapers [44–47]. Disposable adult diapers include both traditional tab and pull-up styles. Disposable diapers have been enabled through cost-effective materials, efficient manufacturing technologies, and the implementation of superabsorbent polymers (SAP).

Incontinence is the loss of either urinary or bowel control, varying from slight loss to complete loss of control [48]. Urinary incontinence can affect all ages, but is most common in older aged adults [49], women after childbirth [50], and men after prostate surgery [51–54].

While urinary incontinence is common, it is surrounded by a negative social stigma [55–58]. Individuals with incontinence are affected in many ways including loss of dignity, decreased socialization, increased depression and stress, and self-consciousness that has adverse effects on quality of life and productivity [59]. The use of adult diapers can be a source of embarrassment and perceived loss of control or independence. Ad campaigns specifically target this consumer challenge by focusing on product secrecy and discretion. To a user, a discreet diaper means a less stressful overall experience, and less impact on their lifestyle [60].

Diapers can provide a physical burden to less mobile users. Diapers are typically compressed in packaging to reduce shipping and packaging costs. The absorbent core in many diapers consists of a fluffy wood pulp/SAP matrix, which stiffens when compressed [60]. Once stiffened into the compressed state, the diaper is more difficult to open and put on. For older adults with poor balance, attempting to put on such a diaper while standing may increase the risk of a fall. These difficulties and risks highlight the need for functions that assist the user in opening or unfolding the compacted diaper.

2.2 Deployable Waistband

A disposable waistband was designed as a means to deploy the diaper once it was removed from its packaging. This deployed diaper waistband would make it easier for users to put the diaper on. When packaged, the waistband is folded and compressed with the diaper; once the packaging is removed, the stored strain energy in the waistband deploys, thereby opening the diaper. While a simple solid band placed into the waistband would open a diaper in this manner, it would not stretch with the fabric to allow an individual to put the diaper on. A waistband system is needed that folds with the diaper when packaged, deploys the diaper when opened, and stretches with the diaper waistband to allow dressing.

2.2.1 Lamina Emergent Torsion Joints

Lamina Emergent Torsion (LET) joints [20] and several LET variants [36–41,61] have been used in many engineering applications ranging from space applications [62–65], to spinal implants [66]. These surrogate folds can be used to replace a standard hinge by cutting designed geometries into adjacent panels. When the LET joint is actuated in a hinge-like motion, the members are torsionally deflected and strain energy is stored. When released, the stored strain energy in the LET joint moves the panels back to their low-energy states.

While the geometry of a LET joint allows a hinge-like motion, it also introduces other undesired motions, referred to as parasitic motions. LET joints can be designed to be flexible in bending and stiff in other degrees of freedom. Such a design replicates hinge-like behavior. While often undesirable in most applications, the parasitic motion observed with a compressive or tensile load could be utilized when elongation along that axis is desired. Pehrson et al. presented a way to design for motion along three degrees of freedom in a LET joint including tension/compression, deflection from in-plane moments, and the desired hinge-like motion [62].

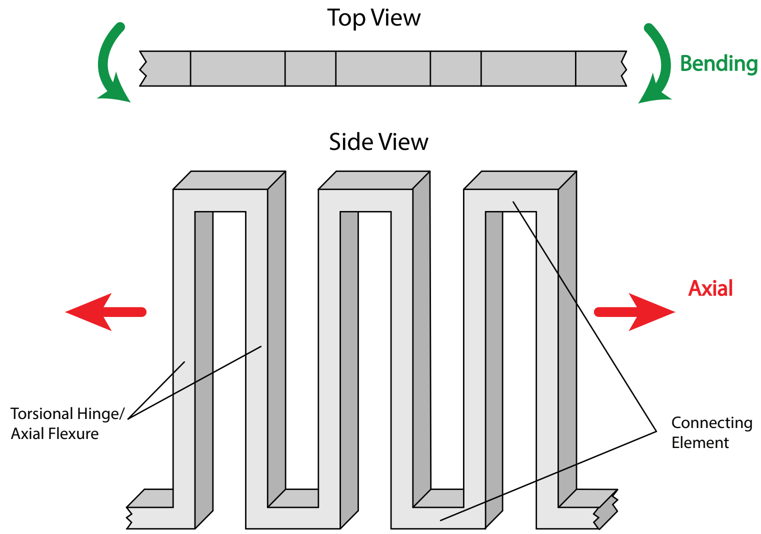

Figure 2.1: Basic elements of a LET Band unit. Displayed are three of the LET Band units that make up the waistband

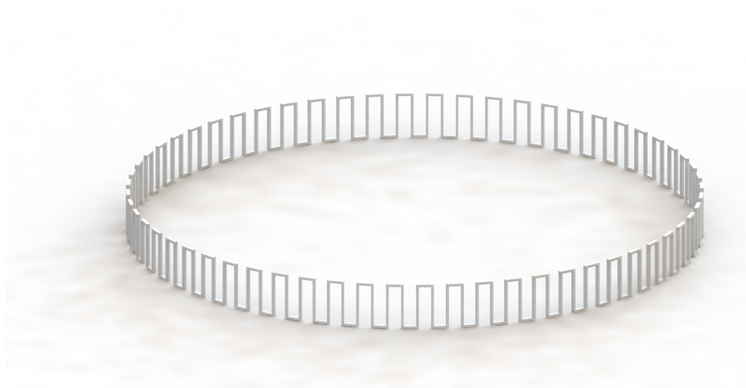

Figure 2.2: Completed LET Band system with a circumference of 28 inches, and dimensions reported in Table 2.1

2.2.2 Proposed Diaper Waistband

A modified LET joint was designed into a plastic waistband as a means to deploy and structure an adult diaper. Similar to the standard LET joint, it is made up of long flexures that can deflect in both torsion and bending. The basic framework of the "LET Band" system is shown in Figure 2.1 and the complete waistband with repeated units is shown in Figure 2.2.

The torsional hinges in a standard LET joint are designed to be flexible in torsion and stiff in bending. This makes the joint as a whole flexible in bending and stiff in tension. This limits the amount of parasitic motion in the joint. In contrast, for use in a diaper, it is required that the waistband stretch with the fabric, and hold the diaper in an open shape. This can be achieved by making the diaper waistband flexible in axial tension, but stiff in bending. This in turn requires the individual flexures in the LET Band units to be flexible in bending and stiff in torsion. As a note, these are opposite to the desired characteristics in a standard LET joint flexure.

Dimensions of the LET Band units can be calculated to maximize the flexure torsional stiffness and minimize the bending stiffness. As shown in [67, 68], the torque of the rectangular cross sectioned flexure can be calculated by

$$T = \frac{\phi G \beta (2h_{flex})^3 (2b)}{L_{flex}} \tag{2.1}$$

where ϕ is the angle of twist, G is the Shear Modulus, L_{flex} is defined as the flexure length, b is defined as the flexure thickness, h_{flex} is the flexure width (see Figure 2.3), and β is a funtion of the ratio b/h which increases to 0.333 as b/h approaches infinity [69].

The torsional stiffness, k_t, can be defined by

$$k_t = \frac{G \beta (2h_{flex})^3 (2b)}{L_{flex}} \tag{2.2}$$

.

As shown by [2], the bending force of a rectangular flexure can be calculated by

$$F_b = \frac{\delta E b h_{flex}^3}{4L_{flex}^3} \tag{2.3}$$

where E is Young's Modulus, and δ is deflection. The bending stiffness, k_b, can be defined as

$$k_b = \frac{E b h_{flex}^3}{4L_{flex}^3} \tag{2.4}$$

To maximize the benefits of the design, the members must maximize the torsional stiffness and minimize the bending stiffness. In other words, minimize the ratio

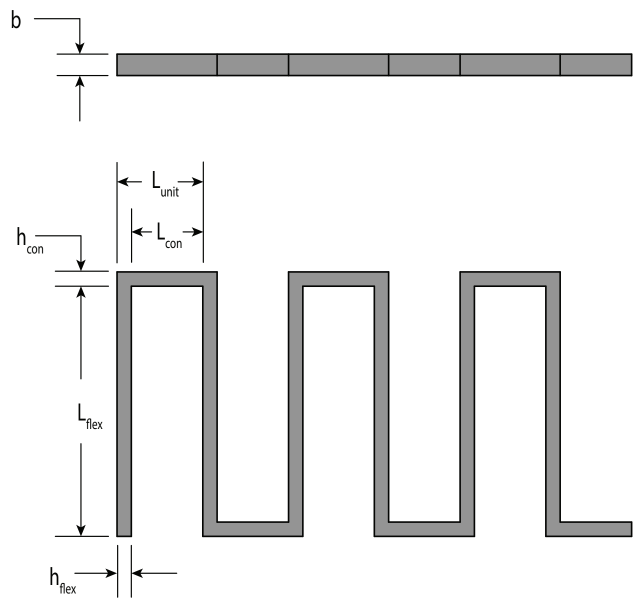

Figure 2.3: General dimensions defined for a LET Band unit. L_{unit} defines the length of each unit while L_{con} defines the connecting element length

$$\frac{k_b}{k_t} = \frac{Ebh_{flex}^3}{4L_{flex}^3}\frac{L_{flex}}{G\beta(2h_{flex})^3(2b)} = \frac{E}{64G}\frac{1}{L^2\beta}. \tag{2.5}$$

Using equation 2.5, we can see that increasing b and L_{flex}, while minimizing h will give us the most favorable design for these requirements.

It is important to note that there is a range of feasible values that can be used in the application of an adult diaper waistband. In other words, increasing b and L_{flex} improves the desired force performance, however the more we increase b and L_{flex} the more uncomfortable it would become to the user. Therefore we must define upper bounds for b and L_{flex} that would ensure a comfortable waistband. For our prototypes and testing, a waistband with b = 1.5 mm and L_{flex} = 17.5 mm were used as those are approximately the corresponding dimensions of a typical leather belt. Dimensional constraints may be changed for desired performance.

After b and L_{flex} are defined, connector length (L_{con}) can be defined using the desired stress in the flexures and the desired axial elongation amount of the waistband. In an adult diaper, the waistband must elongate and increase its circumference to allow the user to put their feet through and pull the waistband over their hips. On a similar note, the undeflected waistband circumference must also be small enough to hold the diaper on the user's waist. The difference between the undeflected circumference (c_u) and the deflected circumference (c_d) two defines how much combined deflection (δ_{total}) the flexures must undergo. Thus

$$\delta_{total} = c_d - c_u \tag{2.6}$$

and the deflection per flexure, δ_{unit}, can be solved using

$$\delta_{unit} = \frac{\delta_{total}}{n_{units}} \tag{2.7}$$

where n_{units} is the number of units. Note that in this waistband design, n_{units} must be even to create a continuous loop. The max stress, σ_{max} in each flexure can be solved by

$$\sigma_{max} = \frac{6\delta_{unit} E h_{flex}}{L_{flex}^2} \tag{2.8}$$

Rearranging we get

$$\delta_{unit} = \frac{\sigma_{max} L^2}{6 E h_{flex}} \tag{2.9}$$

We then can solve for the minimum number of flexures, n_{units}, we need in order to undergo the total deflection without exceeding the max stress.

$$n_{units} = \frac{\delta_{total}}{\delta_{unit}} = \frac{6\delta_{total} E h_{flex}}{\sigma_{max} L_{flex}^2} \tag{2.10}$$

The needed connector length, L_{con}, can be determined to define our geometry.

$$L_{con} = \frac{c_u}{n_{units}} - h_{flex} \tag{2.11}$$

Final dimensions for the LET Band units used in the diaper waistband are reported in Table 2.1.

A prototype waistband was 3D printed from PLA material for implementation and testing. Each waistband was printed in four sections that were connected into final form using cyanoacrylate adhesive.

Prototyped waistbands were sewn into the waistband section of the diaper material to encase the PLA prototype. The completed diaper-waistband prototype was then folded up as it would be in packaging, and then released to observe the waistband's deployment behavior.

2.2.3 Waistband Results

Figure 2.4 shows the prototyped waistband being used in a full diaper prototype in a folded and deployed state. The waistband allowed the diaper to be folded tightly allowing the diaper to be stored compactly. Once released, the waistband moved towards its lowest energy state, forcing the diaper into its opened position.

Once opened, the LET band system exhibited the same elasticity along the waist as the external fabric. In other words, the LET band is able to stretch along its length with the fabric to allow the user to pull the diaper over their hips and conform to the shape of their waist. .

The deployed diaper remained fully open while being supported from one point along the waistband. This suggests that the diaper would remain in its opened shape if the user were to put the diaper on while using only one hand to step into it.

Table 2.1: Final dimensions of the LET band system used for prototyping. Dimensions are dependant on material chosen and imposed comfort constraints.

Parameter	Value (mm)
L_{flex}	17.5
b	1.5
h_{flex}	1
h_{con}	1
L_{con}	7
L_{unit}	12

(a) (b)

Figure 2.4: Integrated waistband prototype in (a) folded state and (b) deployed state

CHAPTER 3. APPROACHES FOR MINIMIZING JOINTS IN SINGLE-DEGREE-OF-FREEDOM ORIGAMI-BASED MECHANISMS

3.1 Introduction

Origami, the ancient art of paper folding, has inspired many engineering designs from many different fields. Deployable origami-based mechanisms can stow compactly and deploy into a large configuration. Deployablilty is achieved through a systematic arrangement of connected panels, or origami arrays. A special category of arrays, origami tessellations, are often used for deployable applications because of their symmetric geometric fold patterns and/or their ability to be repeated linearly or radially.

Deployable origami has inspired designs for areas such as deployable antennas [70–72], medical devices, [73–75], robotics [76], metamaterials [77], and architecture [78]. Deployable origami arrays have also recently gained extra attention when designing reconfigurable antennas as they are inherently physically reconfigurable [14, 26, 79–81].

Designs for these applications generally include mechanisms with many panels and joints to "fold" as origami does. Origami patterns such as the Miura-ori, Tachi-Miura, and twist tessellation patterns have the behavior of storing compactly and deploying to a large area while also having a single-degree-of-freedom (DoF). Single-DoF mechanisms are attractive for such applications because the entire mechanism can be actuated with only one input, thus reducing the number of actuators and the corresponding cost, weight and complexity.

Origami can be modeled as connected sets of spherical mechanisms [82], where each vertex corresponds to the center of rotation of an individual spherical mechanism. These spherical mechanisms, each with a loop constraint, are then connected into a single system of mechanisms by sharing links/panels. The combination of constraints between the individual mechanisms often results in redundant constraints, making the system overconstrained. Multi-vertex origami patterns are overconstrained when at least one hinge is shared between vertices. These redundant constraints have no effect on the intended kinematics of the system when the geometry is assumed to be perfect.

However, when fabricated, imperfect joint axis alignment and placement render the kinematics non-ideal. As a result, these systems can exhibit an increase in unintended resistance to motion or can completely bind during motion. Undesirable internal loads can also result from these non-ideal conditions. In applications such as deployable space arrays, it is vital that the mechanism's actuation force be predictable and minimized. Required forces to actuate these mechanisms could be decreased by reducing the number of joints, particularly when compliant joints (such as flexures, flexible membranes, etc.) are used. It is also important that the mechanism's motion be uninhibited throughout deployment, meaning that it does not bind or meet internal resistance to motion. Deployable space arrays must exhibit reliable and predictable motion, ease of actuation and low unintended resistance to desired motion. Reducing overconstraint in an array by removing redundant joints could lead to improved performance in deployable origami-based space arrays and other multi-loop mechanisms.

Removing redundant joints could lead to additional benefits. Many applications that utilize the foldability of deployable origami arrays such as antennas [12] and solar panels [17–19] seek to maximize usable area once deployed. Joints used to enable the folding motion of the arrays may take up usable area that could be used for communication [83] or power generation, as well as add to the weight and stored volume. Research has been done to reduce area taken up by hinges and the panel gaps created [16]. The elimination of redundant joints would leave more area to be utilized productively and would result in improved performance for deployable space arrays.

The objective of this chapter is to identify overconstraint in origami based mechanisms, and propose techniques to eliminate redundant joints within an array while retaining intended motion.

3.2 Background

To better understand the techniques that will be discussed, we review the fundamentals of origami-based mechanisms. Spherical mechanisms are explained with their connection to origami patterns. General mobility criteria and overconstraint are defined and discussed.

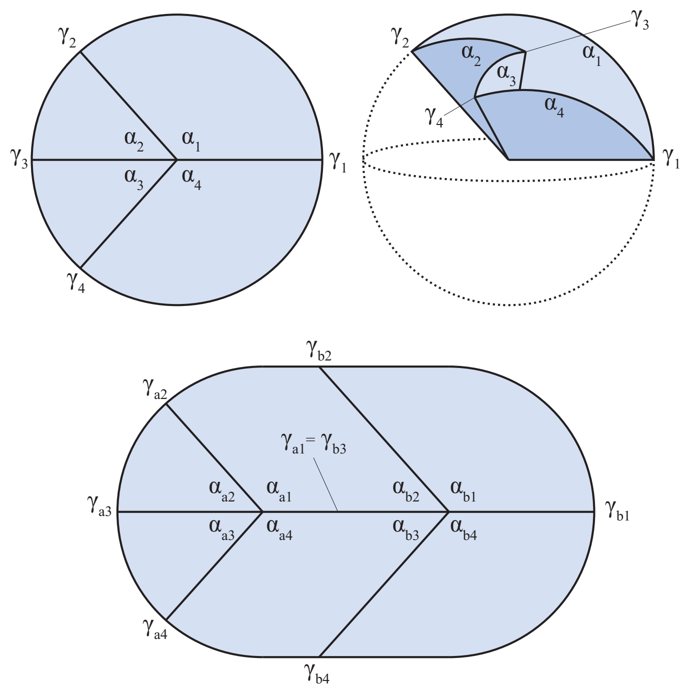

Figure 3.1: Origami vertices can be modeled as a spherical mechanism. Sector angles, α, define the geometry of the origami. Fold angles, γ define fold angles between relative panels. For connected vertices.

3.2.1 Origami and Spherical Mechanisms

A spherical mechanism is a mechanism where all axis of rotational joints point towards and intersect at a specific point in space [84–86]. It has also been shown that an origami vertex can be modeled as a spherical mechanism, and many origami patterns are made up of interconnected vertices or spherical mechanisms [82, 87, 88]. Just as the kinematics of spherical mechanisms are defined by link angles [84], sector angles, denoted by α, define the geometry of an origami vertex. Fold angles, denoted by γ, define the fold angles between relative panels, as shown in Figure 3.1. For a symmetric birds foot, it can be shown that due to symmetry, $\gamma_1 = -\gamma_3$ and $\gamma_2 = \gamma_4$ [89]. For connected vertices, we know that certain fold angles must be the same because panels are shared between vertices. For example, for the degree-4 symmetric birds foot pattern shown in Figure 3.1, panels a_1 and a_4 are the same panels as b_2 and b_3 respectively, thus $\gamma_{a1} = -\gamma_{a3} = -\gamma_{b1} = \gamma_{b3}$.

3.2.2 Mobility of Mechanisms

Mobility (M), also called the degrees of freedom, is used to predict how many independent parameters must be controlled to define the motion of a mechanism. When the mobility is greater than 0 ($M > 0$), the mechanism is "mobile." When the mobility is less than or equal to 0 ($M \leq 0$), the mechanism is considered an immobile structure because there are more constraints than there are degrees of freedom. The development of an equation that predicts the mobility of a mechanism has been researched for over 150 years, with many adjustments proposed over the years [90].

A commonly used mobility equation is the traditional Chebychev-Grubler-Kutzbach mobility criterion, defined as

$$M = \lambda(N - J - 1) + \sum_{i=1}^{j} f_i \tag{3.1}$$

where M = predicted mobility of mechanism, λ = 6 for spatial constraint space and 3 for planar/spherical constraint space, N = number of links, J = number of joints, and f_i = degrees of freedom permitted by joint i.

For a spherical/planar mechanism with only revolute joints, equation (3.1) simplifies to

$$M = 3(N - 1) - 2J. \tag{3.2}$$

For a spatial mechanism with only revolute joints, equation (3.1) becomes

$$M = 6(N - 1) - 5J. \tag{3.3}$$

In the application of origami design, a single origami vertex is a spherical mechanism where axes of the hinges intersect at the vertex [82, 87]. The number of degrees of freedom in a vertex of degree n is $n - 3$ [89]. However, when we look at a multi-vertex origami tessellation as a whole, symmetry and periodicity reduce the overall degrees of freedom. In other words, due to special geometry and redundant constraints, the origami mechanism has more degrees of freedom than Equation (3.1) would predict.

Taking these considerations into account, a few mobility equations for origami-based mechanisms have been proposed. Tachi et al. proposed that for a general bird's-foot crease pattern, such as the Miura-Ori, the mobility can be defined as

$$M = B - 3H + S - 3 - \sum_{k=4} P_k(k-3) \tag{3.4}$$

where B is the number of edges on the border of the pattern, H is the number of holes in the pattern, S is the number of redundant constraints, and P_k is the number of k-gon facets [78, 89].

While traditional mobility criteria would under-predict the mobility of origami mechanisms, this equation takes into account redundant constraints in the system. Despite Equation (3.4) including a term for redundant constraints, S, it can be difficult to identify the exact number of redundant constraints within a pattern. Equation (3.4) is also limited to crease patterns which satisfy the "bird's-food condition." Lang outlined the bird's-foot condition as a vertex with (1) a set of three creases of one fold assignment, separated sequentially by angles strictly between 0 and π, and (2) one additional crease of the opposite assignment [89].

Yu et al. showed that an adjacency matrix could be used to define the number of degrees of freedom in any rigidly foldable origami pattern with multiple vertices [1]. This works very well for traditional origami patterns which include uncut fold patterns. However, once cuts are introduced into the pattern, the adjacency matrix method is limited to single cuts between two vertices, and cannot predict DoF of patterns with holes involving external vertices or more than two internal vertices.

3.2.3 Overconstraint

Mobile Overconstrained Mechanisms

While many adjustments have been made to the original Grubler equation [90], the Chebychev-Grubler-Kutzbach criterion (3.1) can be shown to predict mobility inaccurately for both single [91, 92] and multi-loop systems [90, 93–95]. This inaccuracy is due to overconstraint in the analyzed mechanisms.

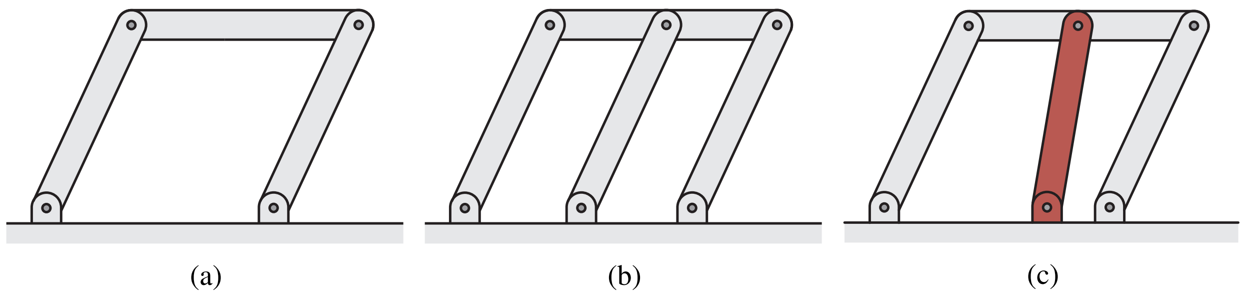

Figure 3.2: (a) Classic 4-bar parallel guiding mechanism. (b) Mobile overconstrained parallel guiding mechanism with redundant parallel link. (c) Immobile overconstrained parallel guiding mechanism due to imperfect joint placement/alignment of one of the links.

Overconstraint is when there exists more constraints than there are degrees of freedom in a system [91, 92, 96, 97]. While overconstraint can mean that a linkage becomes an immobile structure, some special geometric conditions, such a symmetry and angular relations, allow motion even when mobility is predicted to be less than one. A constraint that is redundant can be removed without changing the mobility or motion of the mechanism [98, 99]. A mobile overconstrained mechanisms is one that has more degrees of freedom than is predicted by its mobility equation [91, 92, 96].

For example, the degrees of freedom of the planar linkage system shown in Figure 3.2(a) can be calculated using equation (3.1) as

$$M = \lambda(N - J - 1) + \sum_{i=1}^{j} f_i$$
$$M = 3(4 - 4 - 1) + 4$$
$$M = 1$$

This is defined as an exactly-constrained system, where it is predicted to have a mobility of 1 and is observed to have a mobility of 1.

Now consider the system in Figure 3.2(b) where a link is added and is parallel to the other vertical links. The mobility becomes

$$M = \lambda(N - J - 1) + \sum_{i=1}^{j} f_i$$
$$M = 3(5 - 6 - 1) + 6$$
$$M = 0$$

.

Here, the Chebychev-Grubler-Kutzbach criterion (Equation (3.1)), predicts it to be an overconstrained system with a mobility of 0. However, due to special geometry, this system still has a mobility of 1, and can be classified as mobile overconstrained due to the redundancy in the constraints. We could continue to add more parallel links to the system in the same manner and we would see the predicted mobility decrease, but the actual observed mobility remains the same.

Similar to this planar example, it has been identified that overconstraint is observed in connected spherical systems, such as origami [100]. Tachi showed that any quadrilateral mesh origami pattern is an overconstrained system because the number of constraints around degree-4 vertices (three for each vertex) exceeds the number of variables (the number of hinges) [100]. However, despite being overconstrained, many quadrilateral mesh patterns are still mobile. Similar to planar link redundancy, as shown in Figure 3.2, quadrilateral mesh patterns such as the Miura Ori also have redundant constraints, enabling their motion.

Challenges with Overconstraint

Mobile overconstrained mechanisms often require mathematically perfect geometries. When analyzed assuming perfect geometry, redundant constraints are observed and motion is allowed. However, without perfect geometry, the previously redundant constraints become conflicting constraints and render the mechanism immobile. The conflicting constraints can then limit the mechanism's motion (by locking or binding), cause choppy motion, induce excessive internal loads, and can lead to fatigue failure [101, 102]. For example, Figure 3.2(c) shows an overconstrained planar mechanism that is rendered immobile by imperfect joint placement.

Imperfect geometry can be caused by imperfect tolerancing, imperfect hinge placement, and thermal expansion differences. Clearances can be added into hinge designs to allow enough motion for the joints to line up, even when placed imperfectly [103]. Another approach is to introduce compliance so that the system can flex. While clearances and compliance can allow a mechanism to move in the desired way, it also can introduce unwanted motion in other directions, making the motion less predictable.

In many deployable array applications, it may be beneficial to replace a mobile overconstrained system with an exact-constrained system design to eliminate or minimize these problems.

Specifically, origami-based deployable designs would benefit from the minimization of redundant constraints, and knowing where to remove those constraints.

3.3 Recognizing Overconstraint

While it may be easy to recognize overconstraint in a planar mechanism, it can be difficult to identify overconstraint in spherical mechanisms. The purpose of this section is to provide the reader techniques that can be used to recognize different overconstraints within an origami pattern.

3.3.1 Geometric Overconstraint

An origami pattern containing multiple vertices can be visualized as a system of connected spherical mechanisms, with each vertex within the pattern being the center of its own spherical mechanism. Redundant constraints can be found within multi-loop origami patterns. When individual spherical mechanisms are joined, loop constraints are created and redundant constraints are added. Generally the number of redundant constraints is defined as the difference between the observed mobility and the mobility predicted by the mobility equation [91, 92, 96, 97]. For rigid origami, the mobility criterion can be simplified to

$$M = J - 3V \tag{3.5}$$

where J is the number of internal joints, and V is the number of internal vertices [1]. When special geometry exists, such as symmetry and periodicity, the observed mobility will be larger than that predicted by equation (3.5).

The difference in the observed and predicted mobilities indicates the number of redundant fold angle constraints within the pattern. For example, consider a degree-4 vertex within an origami pattern with a negative predicted mobility. A degree-4 vertex requires one fold angle be constrained to define the position of all panels in the vertex. Loop constraints from adjacent vertices may define more than one fold angle within the degree-4 vertex. Since only one fold angle constraint is required, the redundant constraints may be removed. These are the redundant consraints identified using Equations (3.4),(3.5), and the adjacency matrix method [1].

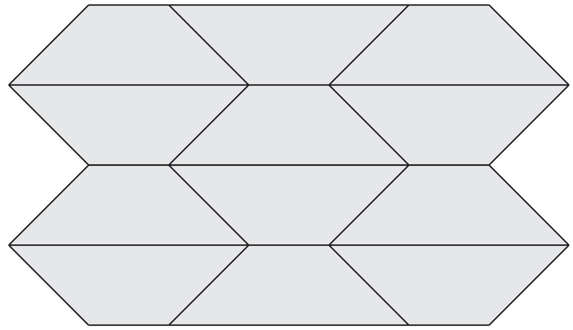

Figure 3.3: Basic 4x3 Tachi Miura folding pattern. Equations (3.4), Equation (3.5), and the adjacency matrix method [1] predict this pattern to have 2 geometric overconstraints (S)

As an example, consider the Tachi-Miura pattern shown in Figure 3.3. Mobilities listed in Table 3.1 are predicted using equation (3.4), equation (3.5) and the adjacency method as presented in [1].

3.3.2 Inter-vertex Spatial Overconstraint

Additional overconstraints can be identified apart from those given by Equations (3.4),(3.5), and the adjacency matrix method [1]. Consider the example of the 2-vertex origami pattern shown in Figure 3.4 taken from a larger origami tessellation. The adjacency matrix method [1] and Equation (3.4) predicts a mobility of 1, with no redundant constraints. Equation (3.2) predicts a mobility of $M = 1$, giving no indication of overconstraint.

However, when we analyze this as a spatial mechanism using Equation (3.3) the mobility is predicted to be $M = -5$, implying some overconstraint. Removing one joint from the mechanism, Equation (3.3) results in a mobility of 0. This implies that while we have removed one

Table 3.1: Predicted mobilities and degree of overconstraint for a 4x3 Tachi-Miura pattern (shown in Figure 3.3 using 3 different mobility criteria. It is predicted that the pattern has 2 redundant geometric constraints

Criterion	**Predicted Mobilty (M)**	**Predicted Overconstraint** (S)
Tachi (Eq 3.4)	1	2
Grubler (Eq 3.5)	-1	2
Adj. Mat. Method [1]	1	2

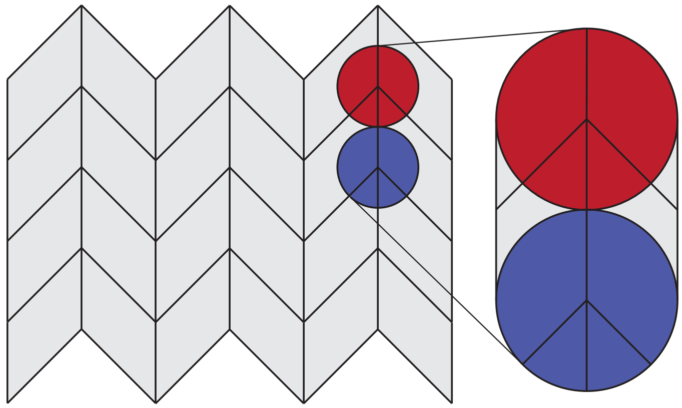

Figure 3.4: Origami can be analyzed as groups of connected spherical joints. The red and blue vertices can be seen as individual vertices with two shared panels.

joint, the mechanism is still overconstrained. Due to panel rigidity and the remaining intact joints, the split edges cannot move relative to each other [104]. This resulting mechanism can be classified as a symmetric double-spherical 6-bar mechanism, which has been shown to be a mobile overconstrained mechanism of mobility 1 [92, 97].

While Equations (3.4),(3.5), and the adjacency matrix method [1] indicated no overconstraint, one hinge between the two vertices is redundant. Due to panel rigidity and the remaining intact joints, the split edges cannot move relative to each other [104].

Visual Representation

It can be difficult to identify this inter-vertex spatial overconstraint. The remainder of this section introduces a visual representation of spherical mechanism constraints in a planar mechanism analogue to visually identify this overconstraint.

Consider two adjacent vertices within an origami pattern that are rigidly connected by two shared panels, as shown in Figure 3.4. For this example, we will use two symmetric degree-4 vertices.

Now consider a special spherical mechanism case where the point at which the axes intersect is infinity. The axes are now parallel to each other, turning the spherical mechanism into a planar mechanism, similar to that done by Wiener [105]. The ratio between sector angles may be represented by a ratio between link lengths. The spherical mechanism in Figure 3.5 (a) can be visualized as a planar mechanism shown in (b). However, we must conserve the angular constraints

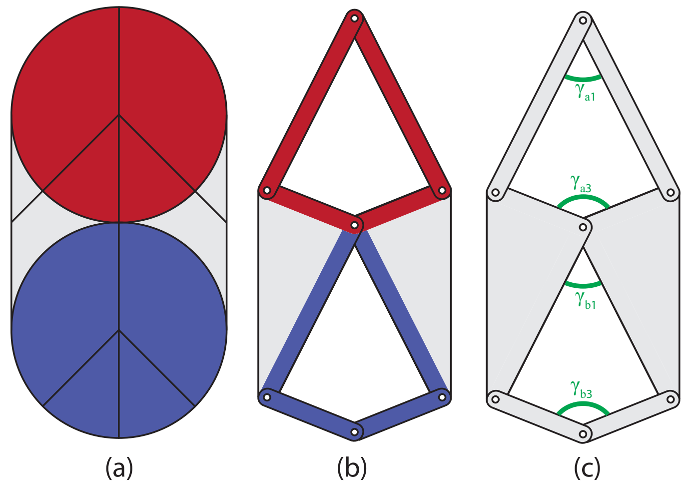

Figure 3.5: (a) Two adjacent origami vertices, which can be modeled as two spherical mechanisms with two shared links. (b) Special case of two spherical mechanisms with axis intersection at infinity. (c) Planar analogue of two connected spherical mechanisms, including angle constraints imposed by original spherical geometry.

exhibited in spherical mechanisms. Because $\gamma_{a1} = -\gamma_{a3} = -\gamma_{b1} = \gamma_{b3}$, we know that the angles between links must follow the same relation.

Maintaining the pin joints and angle relations, the system is overconstrained. If all hinges are placed in their correct locations, motion of the mechanism is not limited. However, consider if the center joint were slightly off-center as shown in Figure 3.6. Physically this could be due to poor manufacturing, poor tolerances, thermal expansion, etc. The previously redundant constraints of the center joint now conflict with the angular constraints, and the mechanism becomes an immobile structure. This can be resolved by removing the redundant constraint, the center pin joint. With the removal of the center joint constraint, the mechanism is still fully constrained.

Applied to the original 2-vertex origami pattern, it is observed that the joint connecting the two vertices can be removed, resulting in the pattern shown in Figure 3.7. This joint is removed while retaining the original single-degree-of-freedom motion.

Figure 3.8 compares this process of identifying redundant constraints between planar mechanisms and spherical mechanisms found in origami.

Although this type of overconstraint is not captured in many mobility criteria, it can be found in multi-internal-vertex origami patterns.

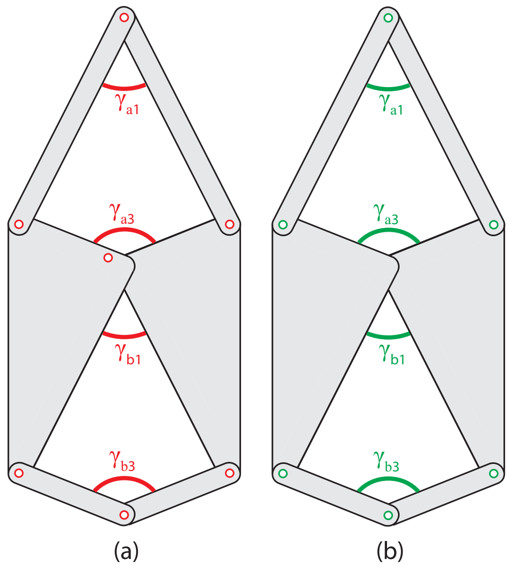

Figure 3.6: Planar analogue for two connected spherical mechanisms (a) shown with conflicting constraints due to improper center joint placement. (b) Removing the center pin joint resolves conflicting constraints while planar analogue remains fully defined.

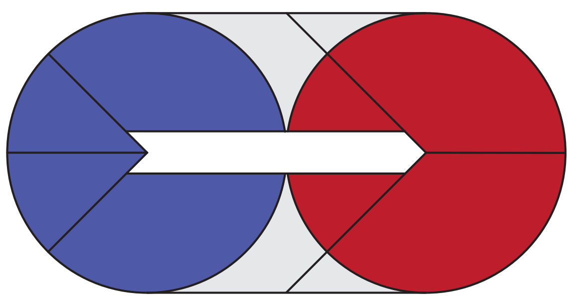

Figure 3.7: Two-vertex origami pattern represented by Figure 3.6(b), with the center joint removed. Observed mobility remains unchanged with the redundant joint removed.

3.4 Techniques to Reduce Overconstraint

This section will introduce various techniques that may be used to reduce geometric overconstraint and inter-vertex spacial overconstraint. Due to simplicity, techniques for the inter-vertex spatial overconstraint will be explained and demonstrated. Then various methods for reducing geometric constraint will be introduced, demonstrated, and discussed.

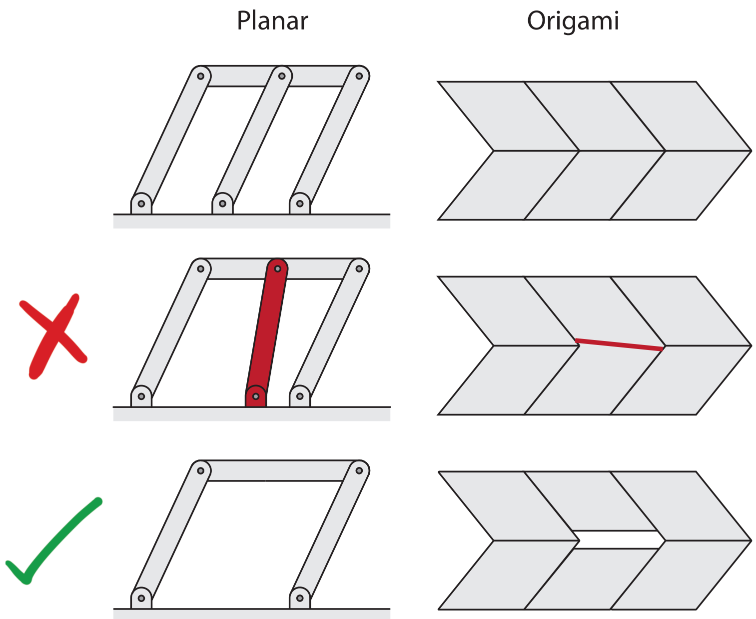

Figure 3.8: Table comparing the visual identification of redundant, and potentially conflicting constraints, in planar and origami mechanisms. Overconstraint can be reduced by removing redundant constraints in the form of links and/or joints.

3.4.1 Inter-vertex Spatial Overconstraint

Because the constraint imposed by the hinge between the two vertices is redundant, the joint can be removed while remaining fully constrained. In addition, removing the joint does not change the mobility due to panel rigidity and angle constraints between vertices. Because the panels in the vertices are rigid and other joints are still in place, edges of the panel where the joint was removed are still kinematically defined and cannot move relative to each other. Figure 3.9 shows a general case of two internal vertices (A and B) where the joint between them can be removed.

Yu et al. calculated the mobility of a "ring pattern with 6 creases," 6 panels, and two local spherical centers from the dimension of the null space of the Jacobian matrix [106, 107], showing it has a mobility of 1 [1]. Essentially, this pattern can be seen as two adjacent degree-4 vertices with their shared fold removed. While this was shown with two degree-4 vertices, this can be extended to vertices of other degrees. Removing the joint between two vertices of any degree does not increase its observed mobility [104].

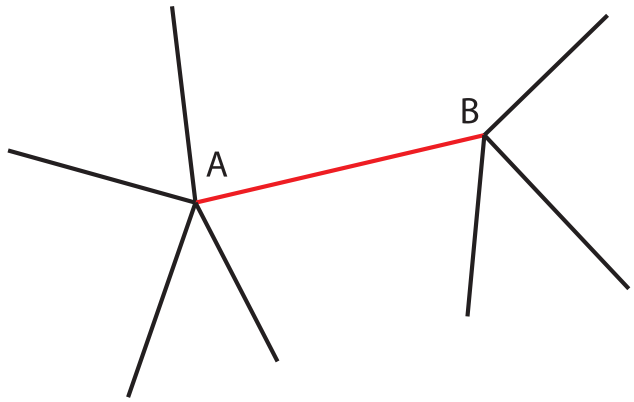

Figure 3.9: Adjacent general vertices, A and B, of any degree, connected by a fold line. The connecting joint (shown in red) is redundant and may be removed without changing the observed mobility.

While not used for the purpose of removing redundant constraints, this single internal joint removal has been has been shown to work in previous research. Lang et al. showed that the center joint is unnecessary in a prototype for a new thickness accommodation technique and its removal can simplify geometry [108]. Single internal joint removal has also been shown to enable motion in a hinge-shifted thick hexagon twist [109].

This can be extended and multiple joints within a large origami array can be removed together. A joint between two vertices can be removed as long as (1) the cut does not touch the edge of the pattern, and (2) cuts do not touch each other. With these conditions, it can be shown that the number of joints that can be removed, R, is

$$R = \lfloor (R^*) \rfloor \tag{3.6}$$

where

$$R^* = \frac{J+1-N}{2} = \frac{V}{2} = \frac{M_3 - M_6}{6}. \tag{3.7}$$

V is defined as the number of internal vertices, M_3 as the mobility estimate from Equation (3.2), and M_6 as the mobility estimate from Equation (3.3).

An example of this is shown for the Miura-ori pattern and a hexagon twist pattern in Figure 3.10. The mobility of these patterns both before and after the joint removal is one. Since any joints can be removed while following these conditions, there may be many permutations of cuts that can

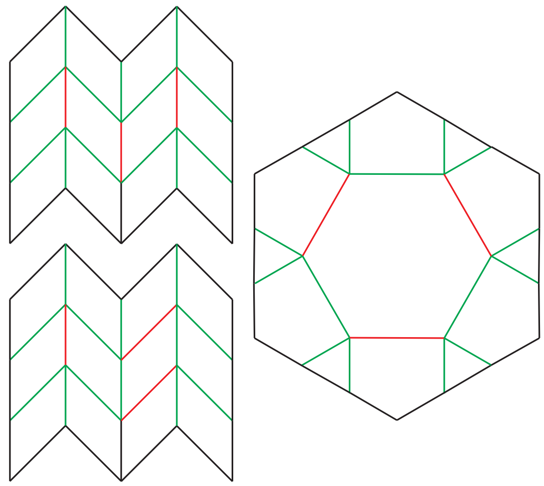

(a) (b)

Figure 3.10: Single internal cut patterns shown for two origami fold patterns. (a)Two permutations of possible single cut patterns in a 1-DoF Miura-ori pattern. Red lines indicate potential joints to be removed, and green indicate intact joints. (b) Possible single cuts for a rigidly foldable, 1-DoF hexagon twist pattern.

be made for a single pattern. For example, Figure 3.10 (a) shows two combinations of cut joints for a Miura Ori pattern.

Prototypes of a thickened Miura-ori and hexagon patterns diagramed in Figure 3.10 were made to demonstrate their 1-DoF motion. Joints were removed as shown in Figure 3.10, and a portion of each panel adjacent to each cut hinge was removed to visually emphasize the hinge removal. The mobility is demonstrated in Figure 3.11 with closed, intermediate, and open configurations.

3.4.2 Geometric Overconstraint

Equation (3.6) calculates the minimum number of cuts that may be made within a pattern without increasing its mobility. The following section outlines techniques that may be used to increase the number of removed joints from a pattern.

Joints Adjacent to Edge

While single joints between two vertices can be removed without increasing mobility, if a joint adjacent to the edge is removed, the mobility prediction increases.

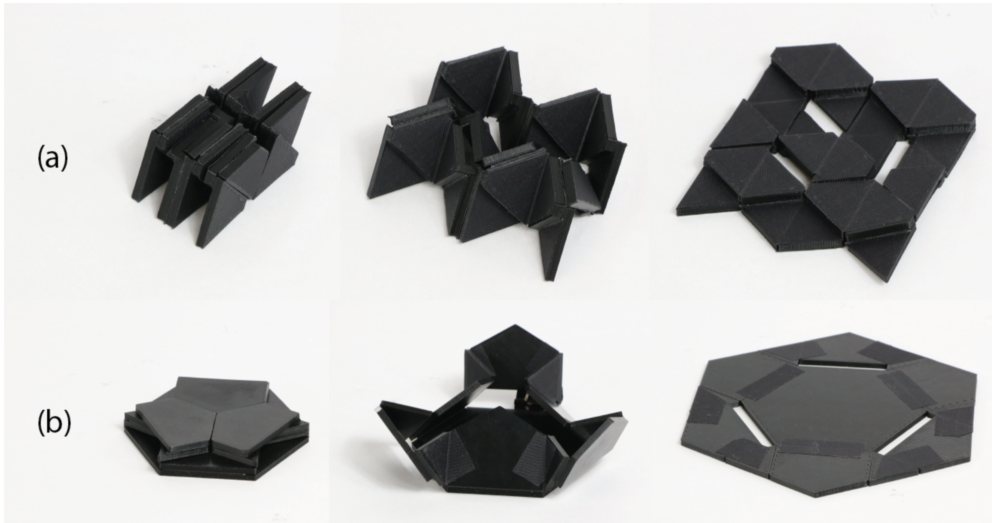

Figure 3.11: (a) Thickened hexagon twist prototype with 3 individual hinges removed around the center panel, as patterned in Figure 3.10(b). (b) Thickened Miura-ori prototype with 3 individual hinges removed as patterned in Figure 3.10(a). A portion of each panel adjacent to cut hinges was removed to visually emphasize the removed hinge location. Each mechanism's kinematics remain unchanged and are shown in closed, intermediate, and open positions.

Yellowhorse et al. showed that this can be used to make immobile rigid folding systems mobile [104]. It was shown that for a group of *n* vertices in a crease pattern, if one crease connecting a vertex to the edge of the pattern is removed, the mobility of the system increases by 2 [104].

Using this technique, we can remove redundant hinges in a mobile overconstrained system. The location of the removed creases is very important to maintain 1-DoF.

When removing joints between two exterior panels, each panel must have at least two additional joints to fully constrain the panels. In others words, any exterior panel with only two connecting joints is not a candidate for joint removal. Any removal of joints would leave the panel with only 1 joint constraint, allowing the split edges to move relative to each other. An example of this is illustrated in Figure 3.12. Location A is not a candidate for removal because that would result in an under-defined panel (highlighted in red) meaning that the panel can move separate from the rest of the 1-DoF system. Location B is a candidate for single joint removal because the separated panels (highlighted in green) are still fully defined through other intact joints.

The predicted mobility and predicted overconstraint for this pattern are shown listed in Table 3.2. For a 3x4 Miura-ori pattern, mobility is predicted to be 1 and it has 2 redundant con-

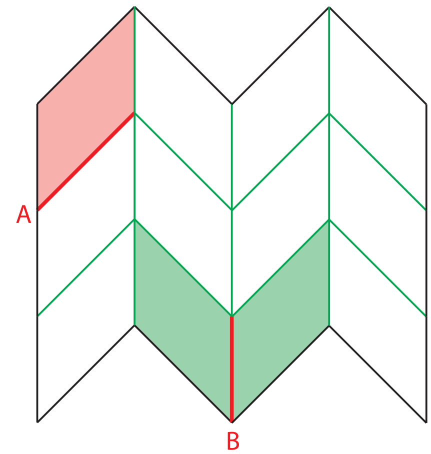

Figure 3.12: Miura ori pattern demonstrating two possible locations of exterior single joint removal. Removed joints are represented by red lines, and intact joints by green lines. A cut at location A would result in an under-defined panel (highlighted in red), meaning it can move separate from the 1-DoF system. The joint at location B may be removed as the split panels (highlighted in green) remain fully defined through intact joints.

straints. After cutting the joint at location B, it can be calculated that the mobility remains at 1, but the overconstraint becomes 0.

Notice that even with the pattern being cut at location "B" and the overconstraint prediction at 0, additional joints can be removed as explained in Section 3.4.1.

Table 3.2: Predicted mobilities and degree of overconstraint for a 3x4 Miura-ori pattern both uncut, and cut at location "B", using 3 different mobility criteria. While the uncut pattern is predicted as overconstrained, the cut pattern is predicted to have no overconstraints.

Criterion	**Predicted Mobilty (M)**	**Predicted Overconstraint** (S)
Uncut		
Tachi (Eq 3.4)	1	2
Grubler (Eq 3.5	-1	2
Adj. Mat. Method	1	2
Cut		
Tachi 3.4	1	0
Grubler 3.5	1	0
Adj. Mat. Method	1	0

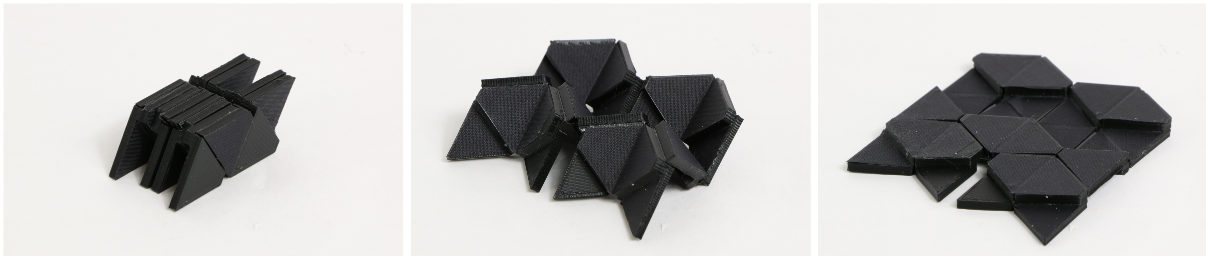

(a) (b) (c)

Figure 3.13: Thickened Miura-ori prototype with an external joint removed. A portion of each panel adjacent to the cut hinge was removed to visually emphasize the removed hinge location. The mechanism's kinematics remain unchanged and is shown in (a) closed, (b) intermediate, and (c) open positions.

A thickened Miura-ori prototype of the pattern in Figure 3.12 was 3D printed from PLA with joints made from spinnaker tape. Only joint location "B" was removed, and was emphasized by removing sections of adjacent panels. The prototype is shown in Figure 3.13. The observed mobility of the mechanism remained unchanged due to the removed joint.

Removing Multiple Joints From Around an Internal Panel

Yellowhorse et al. also showed that multiple creases could be split around a single internal panel as a method to increase mobility of a non-rigid foldable pattern [104]. In a similar manner, we can remove consecutive creases around an internal panel to remove overconstraint while maintaining 1-DoF.

Consider the hexagon twist pattern shown in Figure 3.14(a). Uncut, the mobility is predicted to be 1 with 1 redundant constraint. This overconstraint may be removed by making two consecutive cuts around the center panel, as shown in Figure 3.14(a). It can be difficult to verify the mobility of an entire mechanism without considering sections of the pattern separately. For example, in a single pattern, half of it might be overconstrained while the other may have more than one degree of freedom. However, the overall mobility prediction would not reflect the actual mobility of the mechanism accurately. As such, sections of patterns may need to be analyzed separately for local mobility.

For this hexagon twist origami pattern, sections can be analyzed separately as shown in Figure 3.14(b). The pattern is split by creating a section with panels adjacent to the multi-joint cut.

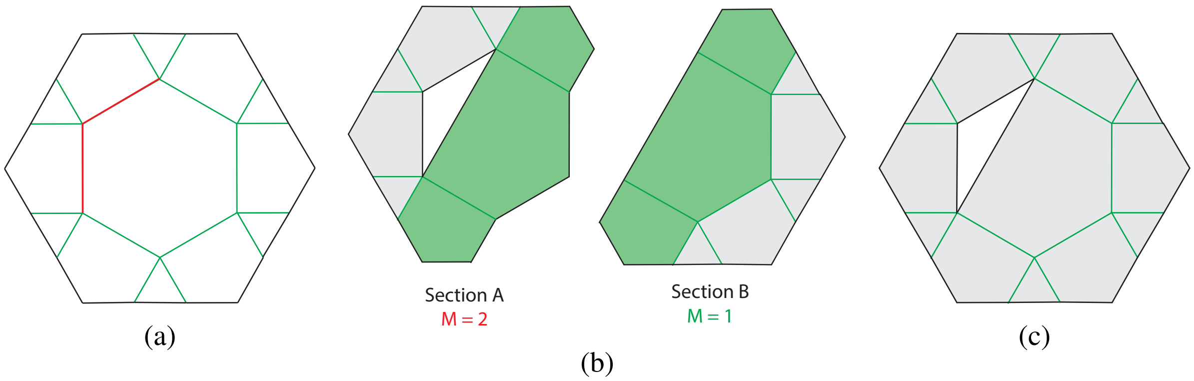

Figure 3.14: (a) Hexagon fold pattern with two consecutive cuts around the center panel. Pattern can be split and analyzed as two separate sections, as shown (b). Green panels indicate panels shared between sections. The resulting 1-Dof system (c), with two consecutive internal cuts around the center panel.

The second section is made from the remainder of the pattern and the connecting panels shared with the first section. For this pattern, it is split into two sections, A and B, each including the shared panels (see Figure 3.14).

Predicted mobilties and overconstraints for the overall uncut hexagon pattern, and each separate section are reported in Table 3.3. We can see that section A is underconstrained, and section B is exactly constrained. When combined into one hexagon pattern, the 1-DoF motion of section B outputs the needed 2 DoF section A requires, resulting in the pattern shown in Figure 3.14(c) with an overall mobility of 1. In other words, the 2 DoF section is driven by the 1-DoF section for an overall mobility of 1.

For this pattern, we cannot cut more than two consecutive cuts around the center panel or it would result in an overall mobility greater than 1. However, it is possible to cut more than two consecutive panels around a single internal panel, as long as the center panel remains defined (with at least two non co-linear hinges), and the separated sections result in an overall mobilty of 1.

A prototype was fabricated to demonstrate the predicted overall mobility of 1. The prototype was made from 3D printed PLA, with joints made from spinnaker tape as a membrane hinge [9]. Because the model has a finite thickness, a thickness accommodation technique is required to enable the motion. For this prototype, the offset panel thickness accommodation technique was used [31]. The assembled prototype can be seen in Figure 3.15. Removed joints are

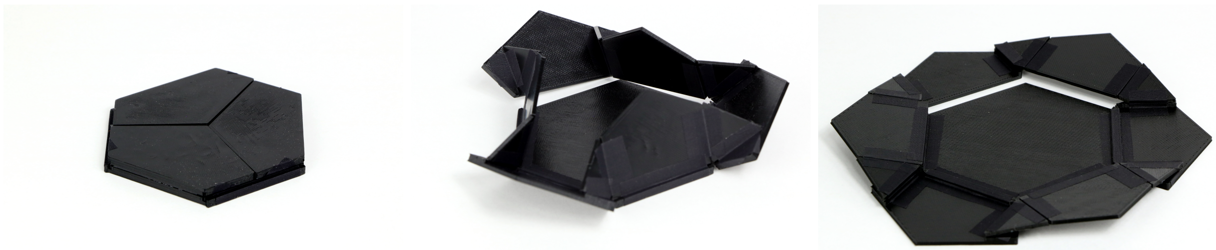

(a) (b) (c)

Figure 3.15: Thickened hexagon twist prototype with 2 consecutive hinges removed around the center panel. A portion of each panel adjacent to the cut hinge was removed to visually emphasize the removed hinge location. The mechanism's kinematics remain unchanged (aside from bifurcation point) and is shown in (a) closed, (b) intermediate, and (c) open positions.

emphasized by large holes in the pattern. While the mobility is 1, it was observed that the mechanism has a bifurcation point midway through the motion.

In addition to removing two consecutive joints, an additional single internal joint between two vertices (as explained in Section 3.4.1) may be removed opposite from the current cut without changing the mobility.

Table 3.3: Predicted mobilities and degree of overconstraint for a hexagon twist pattern both uncut, and cut sections shown in Figure 3.14(b), using 3 different mobility criteria. The uncut pattern is predicted to have an overconstraint of 1.

Criterion	**Predicted Mobility (M)**	**Predicted Overconstraint (S)**
Original Uncut Pattern		
Tachi (Eq 3.4)	1	1
Grubler (Eq 3.5)	0	1
Adj. Mat. Method	1	1
Spatial Section A		
Tachi (Eq 3.4)	2	0
Grubler (Eq 3.5)	2	0
Uncut Section B		
Tachi (Eq 3.4)	1	0
Grubler (Eq 3.5)	1	0

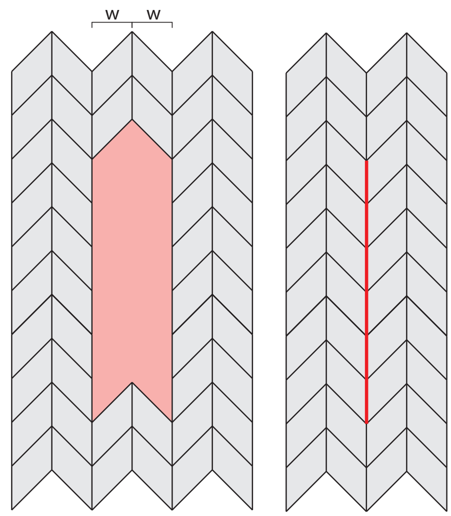

Figure 3.16: Miura mesh with removed panels of width (w), highlighted in red. If panel width of columns containing removed panels is reduced, the removed panels become removed joint constraints.

Removing Joints Traversing Different Panels

It was shown above that it is possible to maintain 1-DoF while removing consecutive joints around a single panel. Similarly, this can also be done while removing several consecutive joints traversing different panels. To maintain 1-DoF while making these cuts, certain conditions must be met.

Connected 1-DoF Sections

Joints may be removed such that it creates multiple separate single degree of freedom mechanisms, while still maintaining enough connections to ensure a mobility of 1 overall.

Beatini et al. showed that entire panels may be removed from Miura-ori patterns to remove overconstraint while maintaining a mobility of 1 [110]. Building on that work, instead of removing entire panels to remove redundant constraints, one could remove the joint constraints between panels using similar rules. A comparison and example of this is shown in Figure 3.16. If the width of rows/columns of the "excessive faces" is defined as W, it could also be analyzed with $W = 0$. The mechanism would still maintain a mobility of 1, but the previously removed panels become removed hinge constraints. This can be done because separate sections of mobility 1 are connected with enough hinge constraints to define the motion with only one overall input.

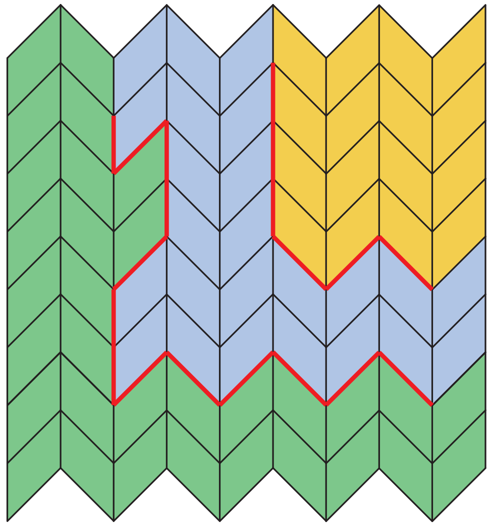

Figure 3.17: Multiple single degree of freedom mechanisms cut from one pattern. Cut joints are shown in red, while intact joints are shown in black. Each separate 1-DoF mechanism is highlighted in a different color. Connectivity between mechanisms ensures an overall mobility of 1.

A similar example using the Miura-ori is shown in Figure 3.17. Notice that this system can be analyzed as multiple smaller mechanisms, each with a single degree of freedom. Sufficient connectivity constraints ensure an overall mobility of 1. Beatini et al. suggested several connectivity guidelines when connecting multiple Miura-ori patterns [110].

This is not limited to the Miura-ori pattern, but can be applied when connecting multiple 1-DoF patterns into a single 1-DoF system.

End-to-End Chains

When cuts are made such that a sections is not 1-DoF, special considerations must me made to ensure an overall mobility of 1.

An end-to-end chain is a sequence of panels where each panel is only connected to two other panels using only two joints. It may be difficult to calculate an overall mobility of a mechanism with an end-to-end chain because part of the pattern may be underconstrained, while an adjacent section is overconstrained. For example, consider the example of the Miura-ori in Figure 3.18. The same number of joints are removed in both patterns, however one guarantees an overall mobility of 1 using the methods from the above section and the other creates an end-to-end chain. The Grubler criterion calculates both of these to have a mobility of 1, however due to special geom-

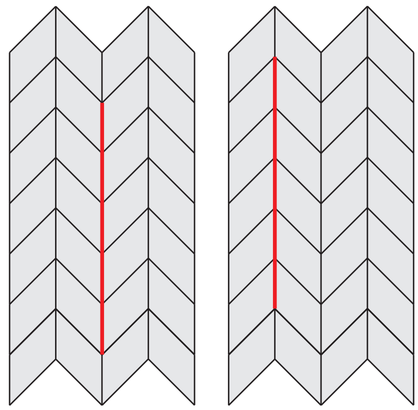

Figure 3.18: Two examples of a Miura Ori pattern, each cut with the same amount of cuts. (a) remains a 1 degree of freedom mechanism, but (b) creates an underconstrained end-to-end chain and increases the mobility of the mechanism.

etry, pattern (b) has a larger mobility. We get this error in the mobility prediction because pattern (b) has a section (the end-to-end chain) with multiple degrees of freedom connected with a largely overconstrained section (uncut section). This is not captured in the mobility criterion.

It may be necessary to analyze sections separately to accurately predict the mobility and overconstraint. One example of this was shown in Figure 3.14.

It is required for an end-to-end chain to have a predicted mobility of 0 to not add an additional degree to the system. For a spherical/planar mechanism with only revolute joints, using Equation (3.2) it can be shown that to not increase the mobility (M=0), N = 3 and J = 3. Thus the end-to-end chain length limit for spherical/planar mechanisms is 2.

For a spatial mechanism with only revolute joints, we use Equation (3.3). In order to not increase the mobility of the mechanism, the end-to-end chain mobility must be 0. It can be shown that for M = 0, N = 6 and J=6, meaning the maximum spatial end-to-end chain length is 5.

It must also be required that a chain must not have more than 3 continually parallel joints, whether consecutive or not. Having 4 continually parallel joints would construct a planar 4-bar, even if non-parallel joints are between these joints. It is important to note that this restriction also applies to 4 spherical joints if the hinges continually intersected at a point. This would result in motion about the spherical center.

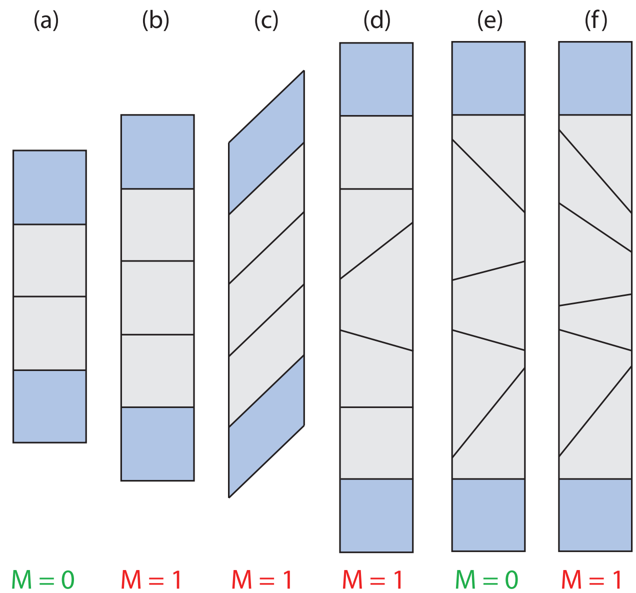

Figure 3.19: Examples of possible end-to-end chains and their mobility predictions if the blue sections' positions were defined. A chain with parallel joints of length 2 (3 parallel joints) is fully defined (a) and does not increase the mobility of the surrounding mechanism. End-to-end chains with 4 continually parallel joints (examples b,c and d) construct a 4-bar, increasing the mobility. An end-to-end chain of length 5 (e) with no more than three parallel joints is fully defined and does not increase mobility. A spacial end-to-end chain of length 6 (f) increases mobility.

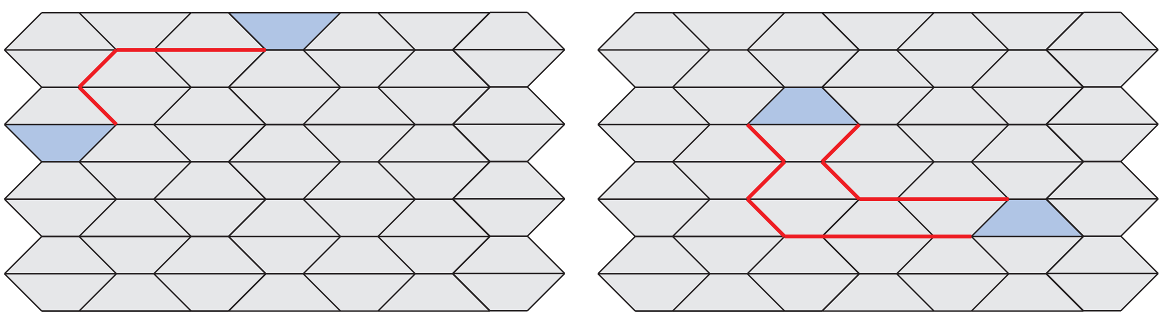

(a) (b)

Figure 3.20: Single cut in a Tachi-Miura pattern, creating an (a) internal and (b) external spatial end-to-end chain of length 5. Both chains do not increase the observed mobility of the overall mechanism.

Figure 3.19 shows various end-to-end chains that may result from pattern cutting. Many of these would introduce an additional degree of freedom, while (a) and (e) would not.

These restrictions enable us to cut joints traversing different panels. An example is shown in Figure 3.20 using the Tachi-Miura pattern. The end-to-end chain created by each cut is a spatial

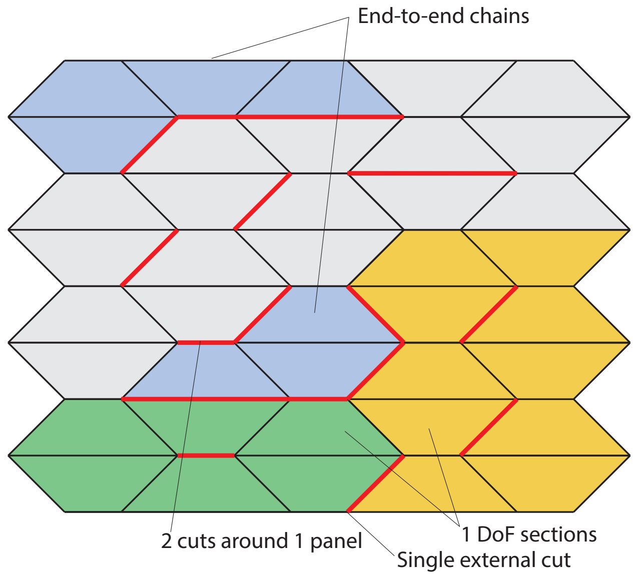

Figure 3.21: Multiple joint removal techniques shown in one Tachi Miura fold pattern. The combined pattern remains 1-DoF despite the multiple removed joints.

linkage of length 5 and does not increase the overall mobility. Note that both chains include only 3 parallel hinges and do not increase the mobility.

3.5 Combination of Techniques

Each of the above joint removal techniques can be combined and used together in a single pattern so long as applicable restrictions described above are followed. Figure 3.21 shows an example of a Tachi Miura with several joints removed using multiple joint removal techniques. Equation (3.6) estimates a minimum of 14 cuts may be removed. By using a combination of techniques, 18 joints were removed in Figure 3.21. Both the uncut and cut versions of this pattern have a mobility of 1. However, the uncut pattern has an overconstraint prediction of 19, and the uncut has a reduced overconstraint of 3. This demonstrates that multiple of the joint removal techniques explained in this chapter can be used within one origami mechanism to reduce overconstraint.

3.6 Discussion

It has been shown that many of these techniques can be used together and can include many permutations of cut-joint patterns for the same origami pattern. While they ensure a mobility of

1 and kinematic properties are similar, it is likely that other properties such as stiffness, actuation forces, and stability may be different for varying permutations. Based on different functional objectives, one permutation might be beneficial over another.

While these methods work to locally identify candidate joints for joint removal, analysis can get complex when removing joints in a large origami pattern. In addition, while these methods can be used to maintain a mobility of 1, they do not inform anything about bifurcation points. For example, while the example shown in Figure 3.14 had a mobility of 1, it was found to have a bifurcation point midway through its range of motion.

These techniques have been shown to reduce the overconstraint of zero thickness origami fold patterns. While many of these can be directly applied to thickened versions of these patterns, some consideration may need to be made when choosing thickness accommodation techniques. For example, when using the split vertex thickness accommodation technique [111], additional folds are introduced. These introduced folds may also be reanalyzed for possible hinge removal.

This chapter has shown how to remove redundant constraints in origami mechanisms without changing its mobility and kinematic behavior. While the non-redundant joints must be left intact, the otherwise removed redundant joints could be replaced for other benefits such as stored strain energy to assist in actuation.

3.7 Conclusion

Single degree-of-freedom origami patterns have proved to be useful in the design of deployable arrays. However, due to an excess of constraints, many origami patterns are overconstrained. Overconstraint introduces many problems to mechanisms when combined with imperfect manufacturing and rigid panels.

This work gives designers a visual and iterative tool that they can use to find alternative joint patterns in 1-DoF systems. The reduction of redundant constraints reduces manufacturing cost, reduces overall pattern stiffness, and reduces the likelihood of binding due to conflicting constraints.

CHAPTER 4. DUAL-PURPOSE LENTICULAR LOCKING HINGE (LENTLOCK) FOR ACTUATION AND STIFFENING OF DEPLOYABLE ORIGAMI ARRAYS

4.1 Introduction

Satellites such as CubeSats utilize origami-based deployable arrays to increase aperture areas of antennas and solar arrays. Folds in these mechanisms are beneficial because they allow a large deployed-to-stowed area ratio. However, once deployed it is necessary that these arrays remain fully unfolded. Due to the folding nature of the mechanism, it can be difficult to prevent the array from re-folding once fully deployed. It is also difficult to assure that each panel is within the required angular tolerances. As an example, reflectarray antenna reception and transmission efficiencies are contingent on the flatness of the panels. Similarly, the performance of deployable optical telescopes depends on the relative alignment of array panels.

This work introduces a compliant hinge design, the LentLock, that can be used to deploy and stabilize foldable arrays. Flexures with geometry based on the Euler spiral, which are included in the hinge design, store strain energy which is used to deploy the system. The out-of-plane motion of the flexures also provide interference which prevents the panels from re-folding. This provides a low-profile solution to joint-deployment and stabilization.

4.2 Background

4.2.1 Deployable Space Arrays

Techniques have been used to enable deployable antennas. Deployable design types include mesh-based [112–116], membrane-based [117–120], inflatable [121–124], and foldable rigid panels [125–127].

Deployable rigid panel antenna designs are used when designing deployable reflectarray patch antennas [27, 28]. Origami fold patterns have been used to enable effective deployment mechanisms to improve stowed-to-deployed area ratios, and simplify actuation through the use of single-degree-of-freedom fold patterns.

All deployable array designs share similar challenges that must be addressed to ensure the performance of the array. Two of the main challenges include a means to deploy the system, and a means to stabilize the system to maintain desired deployed geometry/configuration.

4.2.2 Current Techniques for Array Deployment

Deployable space array designs have employed various deployment techniques [128]. Designs have included inflatable structures [123, 124], perimeter truss systems [114, 116, 129–131], foldable radial ribs [131–133], torsional springs [125–127], root hinges [127], and compliant beams [11]. Rollable booms have also been used to deploy rollable arrays [117, 134–139]. Shape memory polymer composites have also been used in variably stiff tubes designed to deploy flexible solar arrays in a similar manner [140].

State of the art designs of rigidly foldable deployable arrays have included torsional springs and root hinges for hinge actuation [125–127]. However, these designs can include a large part count, high assembly cost, and lubrication. To mitigate these concerns, compliant flexures have been used to replace some or all of the joints within a deployable array [11, 26, 83]. However, these compliant designs can encounter undesirable parasitic motions under loads. In addition, it can be difficult to prevent these designs from re-folding once deployed.

4.2.3 Current Techniques for Array Stabilization

Generally in origami mechanism array design, panel deflection is negligible and panels are assumed to be rigid. In this case, undesired movement and misalignment occurs per the joints themselves. The same folds that enable compact stowage can make it difficult to ensure complete deployment, with panels flat and parallel to each other [109]. With increasing number of individual panels and folds, the potential for compact storage increases, but panel alignment becomes more challenging. This misalignment can be caused by a lack of stability in the deployed state, parasitic joint motions, or external loads.

Various methods have been implemented to stabilize arrays in their deployed state. Techniques at the array hinges have included loaded torsional spring hinges [126], root hinges [127], and systems with springs, cams and gears [141]. Other methods include a cable stayed system [142], cable tensioning [11], and ring truss systems also used for deployment [114, 116, 129–131].

4.2.4 Current Techniques for Combined Deployment and Stabilization

Compliant split tube booms have also been used to deploy and stiffen flexible and rollable solar arrays [134–137]. Shape memory polymer composites have also been used in variably stiff tubes designed to stiffen flexible solar arrays in a similar manner [140].

Strain energy in the form of compliant laminar emergent torsion (LET) joints have also been used to deploy and flatten arrays [83]. Since the low-energy state of these devices occurs when the panels are flat/deployed, the strain energy becomes the means of assuring flatness. However, when fully deployed, the stabilizing forces are only exhibited once deflection loads are introduced, thus small loads can easily misalign the panels.

In a similar way, strain energy stored in torsional springs have been combined with hard-stops to create a more stable deployed state [126, 127]. The energy of the springs deploy the folded panels until the hard stops interrupt the motion at the fully deployed configuration. Designing the lowest energy state of the springs to be past the point of hard-stop interference increases the interference stability. This creates an active stabilization force in the deployed state, as compared to the LET joint stabilization.

Added or embedded lenticular stiffeners have been shown to be effective in stiffening large, thin panels within a pattern [143]. In the same study, Yellowhorse et al. showed that tape springs (lenticular stiffeners) can be placed perpendicular to joints to deploy and stiffen arrays [143].

4.2.5 Euler Spiral

An Euler spiral, also called clothoid spline, is a geometric curve whose curvature changes linearly with its arc length. The Euler spiral also defines the geometric shape of a precurved beam that when cantilevered and loaded vertically at one end would assume a straight line [144].

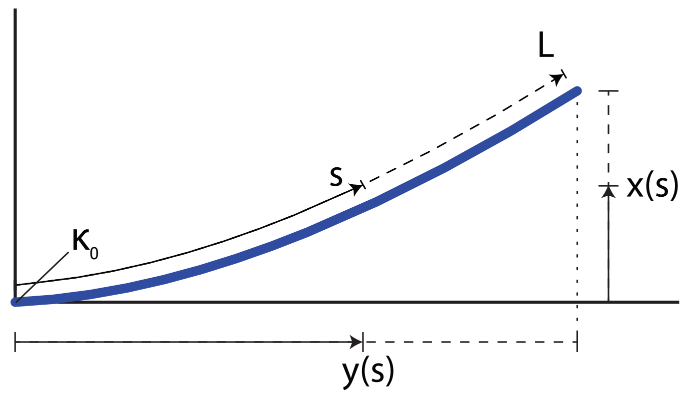

Figure 4.1: Euler spiral flexure geometry and parameter definitions.

Euler spiral geometry has been used in the design of railroads [145–147], nanoantennas and thin film solar cells [148], trajectory planning [149, 150], and for modeling soft robotics [151]. It has also been shown that due to its characteristic of laying flat when under a load, flexures in the shape of an Euler spiral can be used in compact deployable devices [144]. Stiffeners in the shape of an Euler spiral have also been used in the deployment and stiffening of deployable arrays [143]. These Euler spiral flexures are defined as in Figure 4.1, where s is the arc length along the curve, L is total arc length, κ_0 is the initial curvature, and $x(s)$ and $y(s)$ are the coordinate positions.

4.3 The Lenticular Lock (LentLock)

Using the geometry of an Euler Spiral, a joint was designed to both deploy and stabilize folds in an origami pattern. The Lenticular Lock, or LentLock, is composed of two Euler spiral flexures placed parallel to a joint, one on either side. When panels are in their unfolded/deployed positions, the flexures extend away from the panels. In this position, the extended flexures interfere with each other such that the panels cannot fold. To fold the panels, vertical force can be placed onto the LentLock flexures to flatten them against the panels. Then, with the flexures completely stowed, the panels can be folded.

A sequence diagram of a deploying LentLock is shown in Figure 4.2. Figure 4.2(a) shows the LentLock fully stowed, with flexures strained flat and being held in place by a latching force, F_{Latch}. This force could be provided by a latch or burn wire. Once the latching force is removed, the LentLock flexures push against one another, forcing the panels to rotate relative to each other,

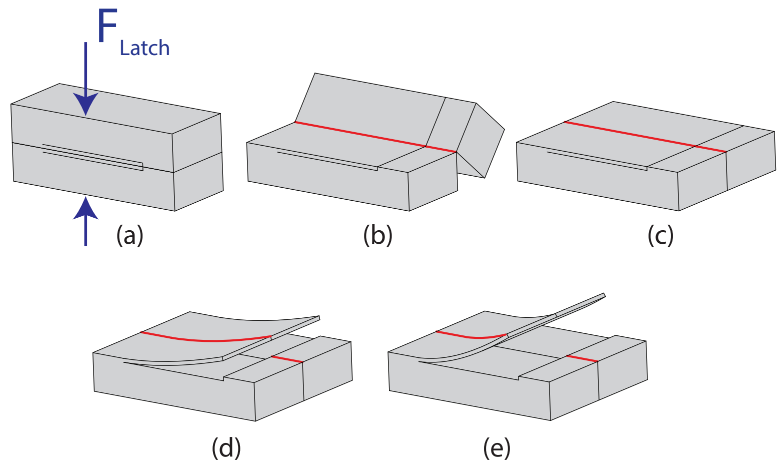

Figure 4.2: A single LentLock fold between two rigid panels shown in several states. Red lines designate hinge lines. F_{Latch} represents the force required to restrain the LentLock hinge from deploying. (a) The stowed state folded with flexures stored. (b) The strain energy in the deflected flexures causes the LentLock to unfold. (c) Panel interference stops rotating motion of panels. (d) The strained flexures begin to deploy, moving away from the panels. (e) Fully deployed LentLock, with extended flexures creating interference to prevent refolding of panels.

as shown in Figure 4.2(b). Once panels are flat, panels interfere and motion stops (Figure 4.2(c)). With the panels flat, the strained flexures can deploy upwards toward their low energy state (Figure 4.2(d)). Figure 4.2 (e) shows the fully deployed joint with LentLock flexures fully extended.

4.3.1 Design

As shown in [143, 144], an Euler spiral curve of length L is defined and approximated as

$$\frac{x(s)}{L} = \approx -\frac{p^5q^2}{40} + \frac{p^4q^2}{8} - \frac{p^3q^2}{6} + p \tag{4.1}$$

and

$$\frac{y(s)}{L} = \approx \frac{p^7q^3}{336} - \frac{p^6q^3}{48} + \frac{p^5q^3}{20} - \frac{p^4q^3}{24} - \frac{p^3q}{6} + \frac{p^2q}{2} \tag{4.2}$$

where

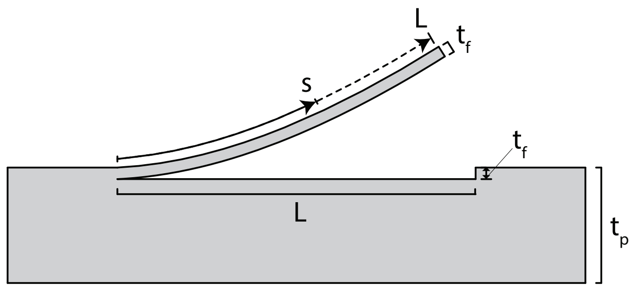

Figure 4.3: Geometry for a LentLock flexure.

$$p = \frac{s}{L} \tag{4.3}$$

and

$$q = \kappa_0 L \tag{4.4}$$

and where κ_0 is the initial curvature.

The geometry of a LentLock flexure is shown in Figure 4.3. Flexures of arc length L and thickness t_f are embedded into a panel of thickness t_p, directly adjacent and parallel to a fold.

Flexure material and flexure thickness (t_f) directly affect the geometry of the Euler spiral curve, and consequently the flexure geometry. Stress equations and limits are outlined in

4.3.2 Actuation

Flexures are fabricated in their deployed state, meaning that strain energy is stored as the flexures are pressed downward, laying flat against the panel. With the flexures flat, the panels can then rotate around the hinge. In this stored state, the strain energy stored in the flexures results in forces pressing against one another, as shown in Figure 4.4. As shown in [143], the force of a flattened Euler spiral flexure is given by

$$F_f = \frac{\kappa_0 b E t_f^3}{12L} \tag{4.5}$$

where t_f and b are the thickness and width of the flexure, respectively.

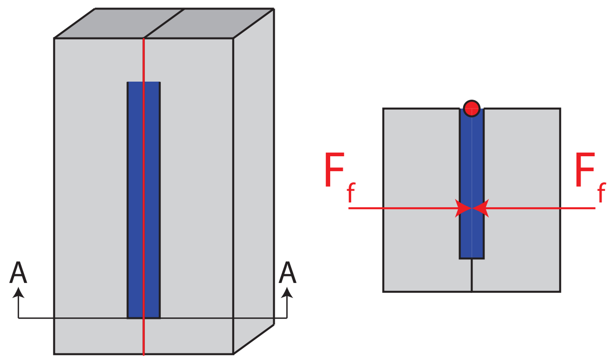

Figure 4.4: LentLock fold shown in its stowed/strained state. The blue area shows the strained flexures, and red lines indicate hinge placement. Flexure forces, F_f, produced by stored strain energy in each flexure, push against one another and open the fold.

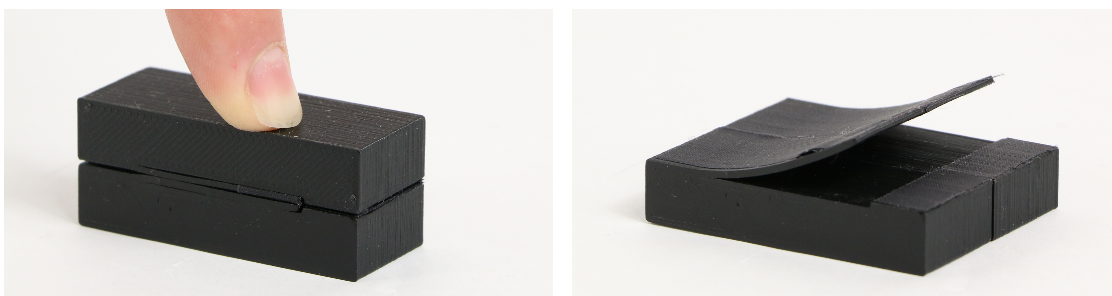

(a) (b)

Figure 4.5: Single LentLock shown in its (a) closed/strained and (b) open/locked positions.

Once the panels are released, these opposing forces push the flexures and panels away from one another, resulting in the panels rotating about the hinge. This energy release actuates and deploys the system.

In Figure 4.5(a), a single LentLock fold is shown folded, held closed. Once released, the LentLock deploys as shown in Figure 4.5(b).

As an actuation demonstration, LentLocks were integrated into the major folds of a degree-4 origami vertex, as shown in Figure 4.6. A thickened version of this vertex was 3D printed from PLA using 5mm thick panels. Thickness was accommodated using the hinge shift method [29, 35]. The prototype is shown in three self-deploying states in Figure 4.7. In this example, two LentLocks, one on each major fold, were used, however additional actuation force and stability against folding could result from additional LentLocks placed on the minor folds.

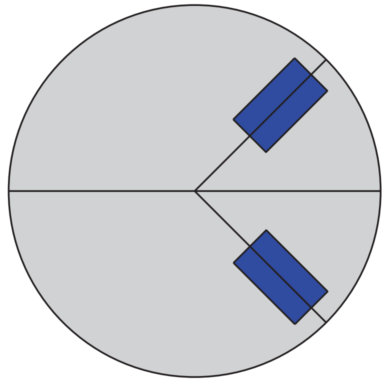

Figure 4.6: Placement of two LentLocks (shown in blue) onto a degree-4 vertex. Here two LentLocks are shown placed on the major folds, however any number of them could be placed on any of the folds.

(a) (b) (c)

Figure 4.7: The LentLock applied to a symmetric degree-4 vertex, with LentLocks on the major folds, shown in its (a) closed/strained, (b) intermediate, and (c) open/locked positions.

4.3.3 Stability

Stability in origami arrays can be achieved through the use of hard stops. When thickness is added to an origami array, panel interference can act as the hard stops to prevent folding toward the panel thickness, as shown in Figure 4.8(a). However, when folding in the opposite direction (away from the panel thickness) there is often no interference to prevent motion (see Figure 4.8(b)).

To add stability to this fold direction, LentLock flexures can be added to the fold. Fully opened panels allow the LentLock flexures to fully extend. The out-of-plane geometry of the flexures creates interference that prevents the panels from re-folding. This interference, combined with the interference from panel thickness gives the system stability by immobilizing the joints in

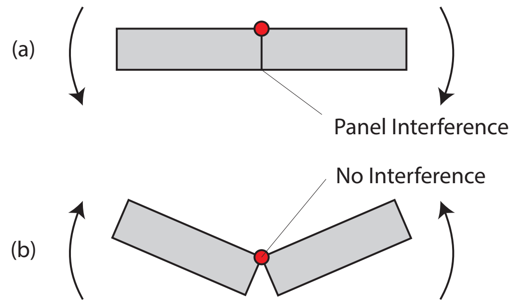

Figure 4.8: Stability from panel interference when actuated (a) toward thickness and (b) away from thickness.

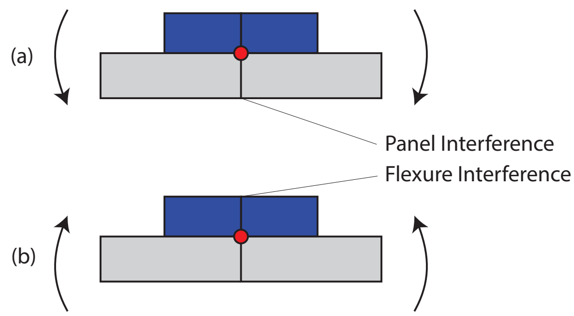

Figure 4.9: (a) Resistance to folding toward panel thickness is achieved by panel interference. (b) Resistance to folding away from panel thickness is ensured by LentLock flexure interference.

both folding directions. The added interference from the LentLock flexures is illustrated in Figure 4.9.

Similar to an increase in moment of inertia, the LentLock flexures add material away from fold-axis, adding stability. While the addition of LentLock flexures stabilizes the joint, increasing the length of the flexure would increase the stability. This is because more material would be placed away from the fold-axis, increasing the stiffness.

To demonstrate the stability added by LentLocks, six-panel z-fold prototype was made with LentLocks on every fold, as shown in Figure 4.10. LentLocks were placed on the valley-fold sides of the joints, meaning that for this example they were placed on alternating sides. A thickened Z-fold prototype was 3D printed from PLA, and assembled using spinnaker tape hinges. The stowed and self-deployed z-fold prototype is shown in Figure 4.11 in an off-loaded configuration (with the hinge axes oriented vertically).

(a)

(b)

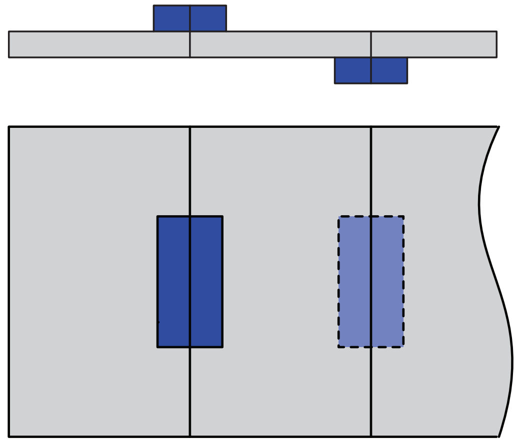

Figure 4.10: Placement of LentLocks (shown in blue) onto a 6-panel Z-fold, shown (a) along the sides of panels, and (b) normal to panel faces. Only the first three panels are shown for simplicity, as the geometry repeats. LentLocks are placed on the sides of the panels where the joint is a valley fold.

(a) (b)

Figure 4.11: LentLocks applied at every fold of Z-folded panels shown in the (a) closed/strained and (b) open/locked positions.

As a comparison, a 6-panel z-fold array was made without LentLocks. Figure 4.12(a) shows both z-fold arrays in their low-energy deployed state. The LentLock array can be seen deployed and locked in its fully extended configuration. In comparison, the simple z-fold remains half deployed and has difficulty remaining fully deployed. When pulled completely straight and released, undesirable folding is still observed in the unstabilized array.

Rotating the prototyped arrays onto their sides (hinge axis now horizontal), the array stiffening exhibited in the LentLock array becomes more apparent. Figure 4.12(b) shows the stiffness of the arrays against their own weight.

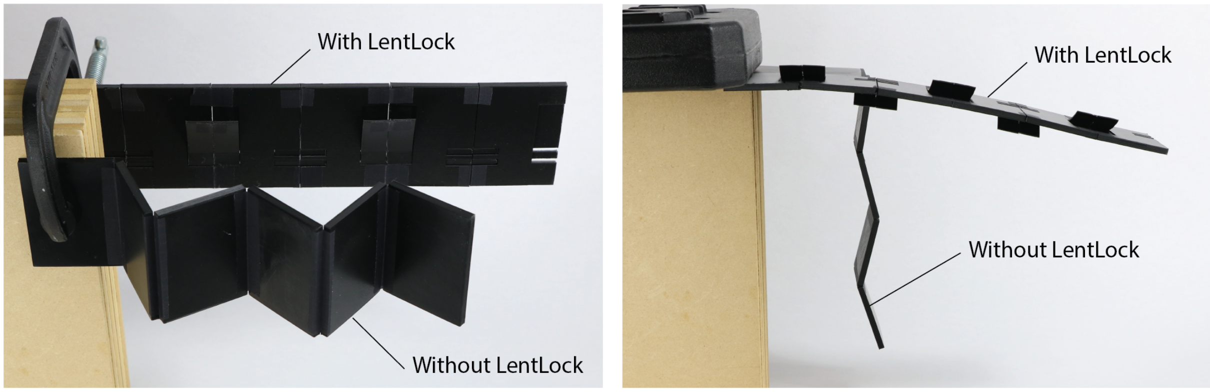

(a) (b)

Figure 4.12: Horizontal stability comparisons to an identical array without LentLocks with hinges arranged (a) vertically, and (b) horizontally.

The combined interferences of adjacent panels and adjacent LentLock flexures prevent the z-fold pattern from folding, stiffening the array against its weight. This shows that LentLocks provide array stiffening at individual joints.

4.4 Pattern Integration

LentLocks may be implemented into full foldable multi-vertex origami arrays as a means to stiffen and deploy the system. For an array with n_m degrees of freedom, n_m LentLocks are needed to completely deploy and stiffen the array. For arrays with multiple single degree of freedom sections, LentLocks must be placed such that each section is deployed and locked.

While only n_m LentLocks are necessary for a system with n_m degrees of freedom, additional Lentlocks increase stability and deployment force.

As a demonstration, LentLocks were applied to a hexagon twist origami pattern, which has been used in deployable systems [152]. Placement of LentLocks are shown in Figure 4.13.

A 5 mm thick hexagon twist prototype was 3D printed with joints made from spinnaker adhesive tape. Thickness was accommodated using the hinge shift technique [35]. Lentlock flexures were arbitrarily chosen to be 1mm thick, with curvature geometry defined such that the PLA does not yield. The prototype is shown self-deploying in Figure 4.14. Once deployed, the LentLocks provide stability and resistance to re-folding. When turned upside down and supported by its center panel, all panels remain fully deployed, as shown in Figure 4.15. As a stability comparison,

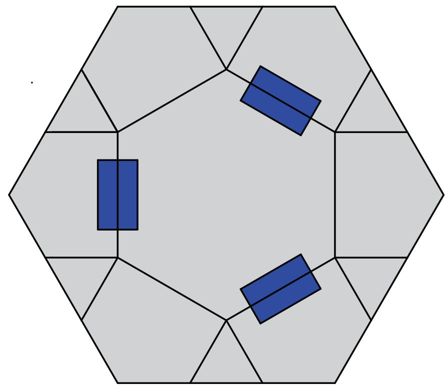

Figure 4.13: Placement of three LentLocks (shown in blue) onto a hexagon twist fold pattern. LentLocks are placed on valley-fold sides of the panels.

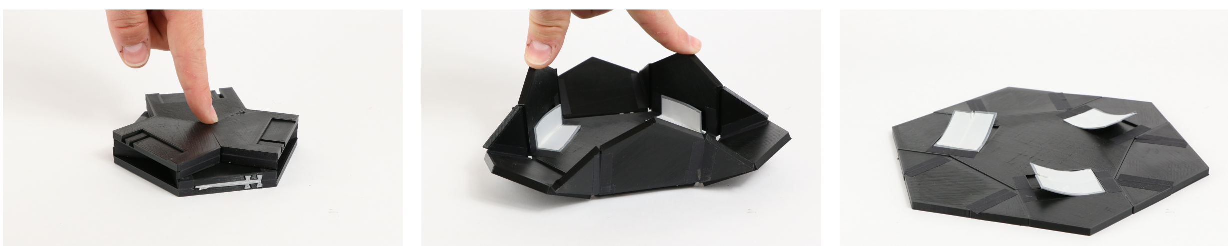

(a) (b) (c)

Figure 4.14: The LentLock applied to a single-degree-of-freedom hexagon twist origami array, shown in its (a) closed/strained, (b) intermediate, and (c) open/locked positions.

the same hexagon twist prototype was made without LentLocks, and is shown held upside down supported only at its center panel in Figure 4.15 (b).

4.5 Discussion

This chapter has shown that LentLocks are a joint-based mechanism that can be used to effectively deploy and stiffen foldable arrays. While these can be placed on any joint within a pattern, they must be placed on the valley-folded side of the joint. This is because the deploying force is perpendicular to the flattened flexures, which can be utilized only on valley folds. In addition, the stiffening from the LentLocks results from their placement opposite from the pane interference. Since panel interference occurs on the mountain fold side of a joint, the LentLock must be placed on the valley side of the joint.

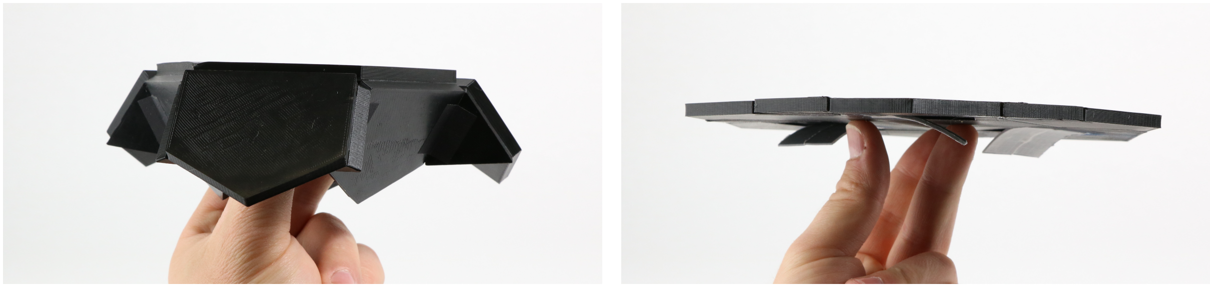

(a) (b)

Figure 4.15: Prototypes of a thickened hexagon twist (a) without LentLocks, and (b) stabilized with LentLocks. Both prototypes are supported at its center panel, with gravity acting to close the pattern. Under its own weight, the unstabilized pattern refolds onto itself, while the LentLock-stabilized pattern remains fully deployed.

While flexures and prototypes were 3D printed for this work, they can be manufactured by other means. Flexures made of composite materials can be laid-up and cured to the correct geometry using an Euler spiral shaped die. Thermoplastics such as PET may be annealed into the correct shape. However, the geometry of the Euler spiral flexures may be difficult to replicate in some materials such as metals without annealing.

For hinges to be placed onto the LentLock flexures, the hinge must be able to deflect with the curvature of the flexures (such as a membrane hinge). However, it is not necessary for the two flexures to be hinged to one another, as the relative panels rotation is defined by hinges between panels. As such, the flexures would be able to deflect independent of each other. With perfect symmetry, the flexures would move together and not slip past one another. However, with imperfect symmetry the flexures may slip past each other and result in incomplete deployment and no locking. To ensure flexure alignment and synchronized deflection, a joint between the flexure tips is beneficial.

4.6 Conclusion

Foldable, deployable arrays enable large planar structures such as antennas and solar arrays to be folded and stored compactly. Consequently, efficient folding patterns allow for increasingly larger arrays, resulting in higher gains and power for spacecraft. While foldable arrays facilitate these benefits, they can be difficult to deploy. In addition, the same folds that enable the motion become a challenge once in the deployed state as the array may continue to fold when undesired.

In this chapter LentLocks were introduced as a joint-based mechanism used to deploy and stabilize foldable arrays. Strain energy from deflected Euler spiral flexures provide the energy for pattern deployment. Once deployed, flexures provide interference to prevent the array from refolding. LentLock performance was demonstrated using various folding patterns and prototypes.

CHAPTER 5. JOINT SELECTION AND INTEGRATION INTO DEPLOYABLE ORIGAMI ARRAYS

5.1 Introduction

The folding motion in any foldable array is made possible through its joints. A joint is a part of the array around which adjacent the panels can rotationally articulate. This chapter is a collection of thoughts which a designer may utilize when choosing joint types for an array design, or to consider alternative options to standard joints. Joints considered will focus on compliant joints. This chapter also discusses how individual hinges have been combined into hybrid joint systems with beneficial behaviors.

Joints such as a traditional pin-joint hinge are often used because of they are simple to apply and involve very little extra design work. However, there are many joint types that offer benefits to certain design circumstances, such as electrical continuity, monolithic design, or stored strain energy that can be utilized for deployment.

Some of these joint types include: Lamina Emergent Torsional (LET) joint [20], variations of the LET joint [36–41], membrane hinge [9], CORE joint [21, 22], ReCS technique joint [23], hinges including tape springs [16, 143, 153], and many more [33, 42, 43].

5.2 Joint Characterization

Each joint type offers benefits and drawbacks which are defined by the desired joint behavior. In other words, the desired behavior defines whether a certain aspect of a joint's behavior is beneficial or poor. For example, a LET joint [20] is useful because it stores strain energy that could be used in an array for self-deployment. The LET joint also enables a very large range of motion. However, this joint is very liable to parasitic motions, or undesired motions, and generally cause adverse effects in a design. On the other hand, whether or not a motion is desired or parasitic depends on the application. For example, work published by Pehrson et al. showed that motions

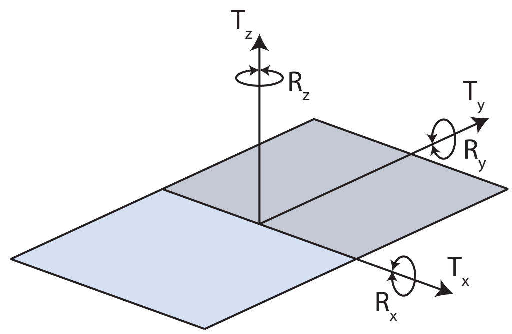

Figure 5.1: Translational (T) and rotational (R) parasitic motion directions between two relative panels.

that are generally thought of as parasitic actually made the pattern's motion possible [11]. In this case, the off-axis motion is desirable.

While the above joints have been characterized individually, no comparison between many relative performances has been compiled. This would allow a designer to consider joint types which exhibit behavior similar to those desired for a specific application. The following metrics were chosen and defined to enable comparison of joint types and characteristics.

R_x **Range of Motion** - Describes the general amount of angle deflection the joint can undergo. While specific geometry within a joint design defines the deflection performance, this metric is meant to offer the designer a potential deflection ranges.

Resistance to Degrees of Freedom - This indicates a joint's inherent resistance to relative transitional and rotational motions. A rating of "+" designates a strong resistance to motion in that direction. "0" indicates marginal resistance to motion, and "-" represents low resistance to motion. Directions for each degree of freedom is defined in Figure 5.1, and are demonstrated in Figure 5.2.

Design Complexity - Indication of the relative difficulty of joint implementation into thick-folding patterns. "Low" indicates a joint that can be applied between two rigid panels with little-to-no computations. A "high" design complexity indicates a joint that requires many geometric and material considerations and may require extensive calculations.

Backlash - Indicates whether motion can be lost due to gaps or clearance between parts.

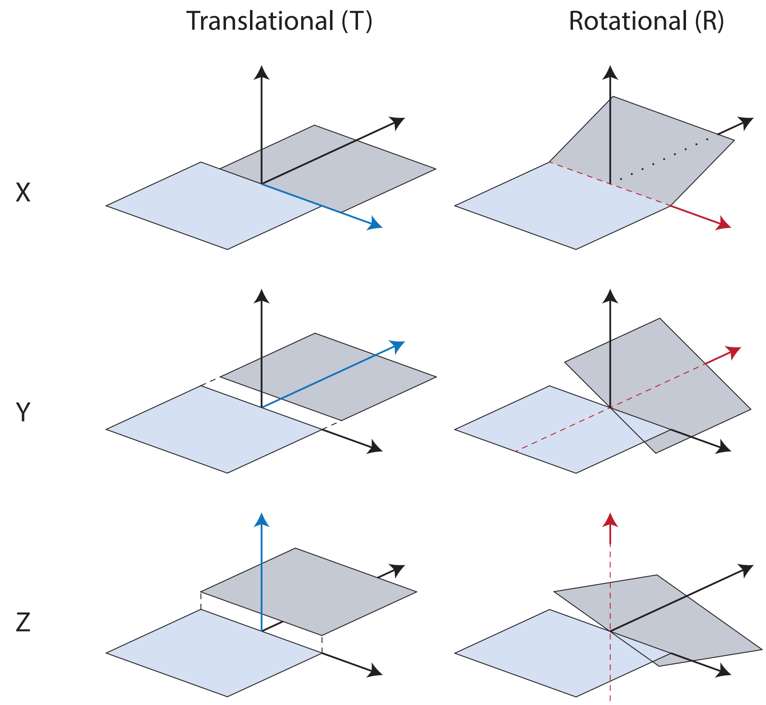

Figure 5.2: Translational (T) and rotational (R) parasitic motions demonstrated between two panels. Blue arrows indicate direction of translational motion, and red dotted lines indicate axis around which rotations are made.

Electrical Continuity - This refers to the inherent potential of the joint type to carry electrical charges across the joint. This includes continuous components that traverse the joint between panels.

Monolithic vs Assembled - This metric describes whether the joint type has potential to be used in a monolithic design, meaning the joint and surrounding panels are all one part. Assembled refers to a joint that has multiple parts and must be assembled into the final joint.

Strain Energy - This indicates whether the joint stores strain energy that may be utilized for deployment or stability. This also indicates potential resistance to motion due to elements in the joint being strained.

Means of Stability - Describes the potential means of stability, if any, provided by the joint. This includes panel interference characteristic of the joint (P), low-energy stable strain states (S), or geometric changes (G) such as moment of inertia changes (as seen in tape springs).

Using the above metrics, each joint was characterized and summarized in table 5.1.

Table 5.1: Comparison table of joint performances and characteristics, focusing on basic compliant joints. Legend for each metric can be found in Section 5.2.

Joint Type	R_x Range	Resistance to DoF							Design Complexity	Backlash	Electrical Continuity	Monolithic/ Assembled	Strain Energy	Stability
Pin Joint	$\pm180°$	+	+	+	+	-	+	+	Low	Y	N	Assembled	N	-
Root Joint [16]	$< \pm180°$	+	+	+	+	-	+	+	Low	Y	Y	Assembled	Y	G,S
Membrane (Line) [9]	$\pm180°$	+	+	+	+	-	+	+	Low	N	N	Assembled	N	-
Membrane (Gapped) [9]	$\pm180°$	0	+	-	-	-	-	-	Low	Y	N	Assembled	N	-
Living Hinge	$\pm180°$	+	+	+	+	-	+	+	Low	N	N	Monolithic	N	-
SLFP [2]	$< \pm45°$	+	+	+	+	-	0	0	Low	N	N	Monolithic	N	S
LET [20]	$> \pm180°$	0	-	-	-	-	-	-	Med	N	Y	Monolithic	Y	S
M-LET [38]	$> \pm180°$	+	+	0	0	-	0	0	Med	N	Y	Assembled	Y	S
T-LEJ [37]	$< \pm90°$	+	+	0	-	-	0	0	Med	N	Y	Monolithic	Y	S
I-LEJ [37]	$< \pm90°$	+	0	+	-	-	-	0	Med	N	Y	Monolithic	Y	S
OD-LEJ [39]	$> \pm180°$	-	0	0	-	-	-	0	Med	N	Y	Monolithic	Y	S
IT-LEJ [37]	$< \pm90°$	+	+	+	0	-	-	0	Med	N	Y	Monolithic	Y	S
CORE [21,22]	$\pm180°$	+	+	+	+	-	+	+	Med	N	Y	Assembled	Y	S
Degree Offset [43]	$\pm180°$	+	+	+	+	-	+	+	High	N	N	Assembled	N	-
ReCS [23]	$+180°$	+	-	-	-	-	-	-	High	N	Y	Assembled	Y	S,P
Volume Trimming [42]	$< +180°$	+	+	+	+	-	+	+	High	N	N	Assembled	N	P
SORCE [33]	$\pm180°$	+	+	+	+	-	+	+	High	N	Y	Assembled	N	-

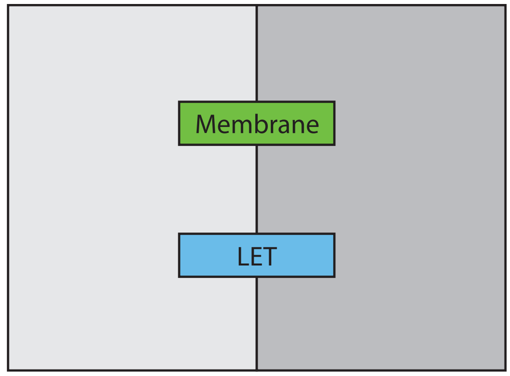

Figure 5.3: Symbolic representation of a membrane-enhanced LET joint. Components include a LET array used for strain energy storage and hinge motion, and a membrane used to limit the parasitic motions of the LET array.

5.3 Hybrid Joint Patterns

As shown, individual joints exhibit specific behaviors, including both desirable and undesirable characteristics. Using a combination of multiple joints within a single folding mechanism can bring additional benefits.

5.3.1 Single-Fold Hybrid

A single-fold hybrid is one that utilizes the characteristics of multiple joint types within a single fold. This is often done to lessen the undesired characteristics of a joint type (such as parasitic motions), or introduce a desirable behavior (such as storing strain energy).

One example of a hybrid joint is the membrane-enhanced LET joint [38]. This joint proposed by Chen et al. combines two joint types into one, utilizing the benefits of both. While LET arrays store strain energy that can be used for deployment, they often suffer from parasitic motions. While the membrane hinge has limited parasitic motions, it cannot store strain energy. Being placed onto the same hinge in parallel, benefits from both joint types are utilized. A symbolic representation of this is shown in Figure 5.3.

The MarCO used custom wing-style hinges with torsional springs to deploy panels of a high-gain reflectarray antenna [154]. The MarCO also implemented root hinges as a means to deploy, orient, and stabilize the array into its desired direction [16]. Root hinges comprise of a pin-style joints combined with strain storing tape spring flexures. Functionally, a root hinge can

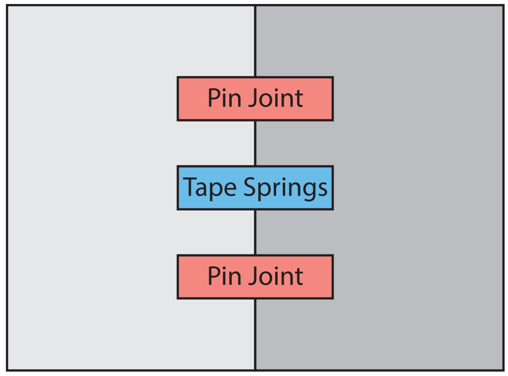

Figure 5.4: Symbolic representation of a root hinge. Components include a tape spring used for deployment and stabilization, surrounded by pin joints used to define the kinematics.

be analyzed as a hybrid joint with two joint types along the same fold, as shown in Figure 5.4. The pin-style joints ensure the desired kinematics but cannot self-deploy. The tape springs do not provide a reliable hinge motion, but provide the deploying force and stabilization to the fold.

5.3.2 Hybrid Joint Array

A hybrid joint array is an array with only one joint type per fold, but multiple joint types within the array.

An example of this was demonstrated by Pehrson et al. in a self-deploying self-stiffening and retractable (SDSR) flasher array [11]. The SDSR design implemented both pin joints and LET joints. Pin joints were used in hinge locations that required large rotations. LET joints were used to both enable motion through parasitic motions, and as a means to deploy the system through stored strain energy. A symbolic representation of this joint arrangement is shown in Figure 5.5.

5.4 Pattern Integration

Hybrid joint array design can benefit from the research presented in Chapter 3. The joint minimization techniques explained in Chapter 3 are used to identify and remove redundant constraints in origami mechanisms without changing its mobility and kinematic behavior. While the non-redundant joints must be left intact, the otherwise removed redundant joints may be replaced for other benefits such as stored strain energy to assist in actuation.

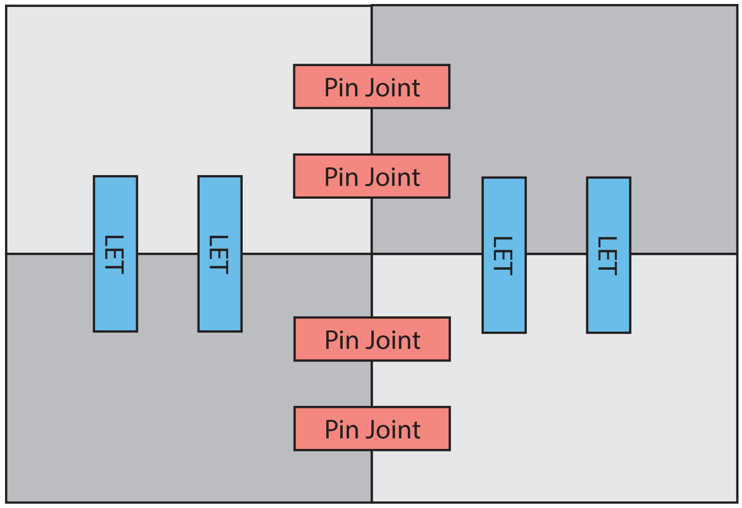

Figure 5.5: Symbolic diagram of joint functions exhibited in the self-deploying self-stiffening and retractable flasher design presented by Pehrson et al. [11]. Joint types include pin joints for hinge locations with large rotation requirements, and LET joints to deploy the system.

LET joints and LET joint variants have been used to actuate folding deployable arrays. Typically, LET joints are used as both a hinge and a means to store strain energy. As a hinge, loads can deflect the LET joints into undesired parasitic motions causing the array to deviate from the expected kinematic motion. As a means to store strain energy, LET joints can be utilized as a means to actuate a deployable array.

Using the techniques explained in this work, the kinematic motion of an origami array can be defined using only a percentage of the array's joints. Instead of removing the identified redundant hinges, these may be converted into a means to deploy the system by changing these joints to strain-storing joints, such as the LET joint. While these replaced joints will not be required to ensure the expected kinematic motion, they will store/release strain energy while following the defined motion.

Consider the hexagon pattern in Figure 5.6(a). It was shown in Chapter 3 that the joints in red may be removed without changing the mobility of the system. Instead of removing these joints, they can be replaced with strain energy storing joints such as LET joints. This creates a hybridized array of kinematic and strained joints. The ”kinematic” joints ensure the single degree of freedom motion, and the ”strained” joints deploy the system.

Figure 5.6 shows a diagram of the hexagon pattern with replaced LET joints. A demonstration prototype was fabricated using 3D printed PLA, and is shown in Figure 5.7. The intact

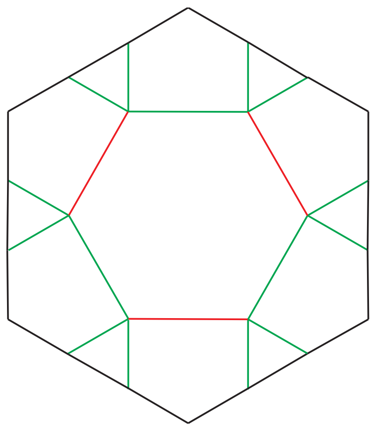

(a)

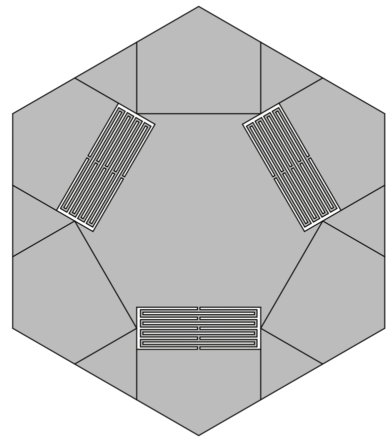

(b)

Figure 5.6: (a) 1-DoF hexagon twist fold pattern with multiple single joints removed, as explained in Chapter 3. (b) Diagram showing the same hexagon twist pattern, but with redundant hinges replaced with LET joints for strain energy storage.

(a)

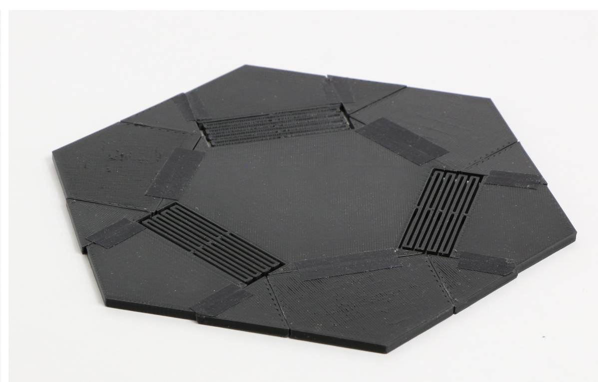

(b)

Figure 5.7: Hexagon pattern with LET joint replacements, shown in both (a) closed/strained, and (b) deployed/released states. Motion of the array is fully defined by the membrane joints. While LET joints can be used as hinges in an array, the sole purpose of the LET joints in this design is to store and release strain energy.

membrane joints, made from spinnaker tape, ensure the predicted motion while the LET joints store enough energy to deploy the array. Note that again, the motion of each panel is the same as the un-cut version.

5.5 Conclusion

When designing origami-based arrays, various joint types can be used to produce relative panel motion. Because each joint type has a specific behavior, a designer must evaluate which joint type to use in an array. While some ensure very little parasitic motions, others provide strain energy that can be used for deployment. This section has used various metrics to compare joint performance and has summarized the characterizations into a table which designers can use when selecting joints.

Combining multiple joint types either onto a single fold, or within an array can produce beneficial behaviors. It was demonstrated that while some joints may be used to define kinematics, other types can be used within the say array to deploy the system.

CHAPTER 6. DEPLOYABLE ARRAY CASE STUDIES

6.1 Introduction

This chapter will discuss multiple case studies in which foldable origami mechanisms were designed to ensure predictable, reliable, and repeatable motion for deployable reflectarray antennas. Designs include a monolithic reconfigurable RA, and foldable RA's based on the straight major square twist and augmented square twist origami fold patterns. Design of each RA included thickness accommodation technique selection, hinge selection, and RA patch antenna implementation. These sections are based on contributions to select publications [26–28].

6.2 Monolithic Foldable Reflectarray Enabled Through Surrogate Fold

A physically reconfigurable RA that exposes multiple apertures was designed for CubeSat applications. Depending on the fold configuration of the RA (as shown in Figure 6.1) different panels are exposed and different antenna behavior is achieved. For example, the folding design shown in Figure 6.1 allows for four distinct RAs: two different pencil beam antennas, and two different dual beam configurations. In other words, this work presents a physically reconfigurable antenna with beamstearing capabilities and multiple antenna apertures. Surrogate hinges were designed and optimized to enable the folding motion and deployablility of the RA.

6.2.1 Surrogate Hinges

Two surrogate hinges are introduced in the design to make the RA foldable as shown in Figure 6.1. These surrogate hinges are realized by making slots on a single piece of thick, rigid material (in this case, PCB). The slots create LET joints that allow the rigid structure to rotate around the axis of the hinges by placing the long segments of the joints into torsion. The hinges are appropriately designed to bend $\pm 180^{\circ}$, while maintaining mechanical integrity. Placing these

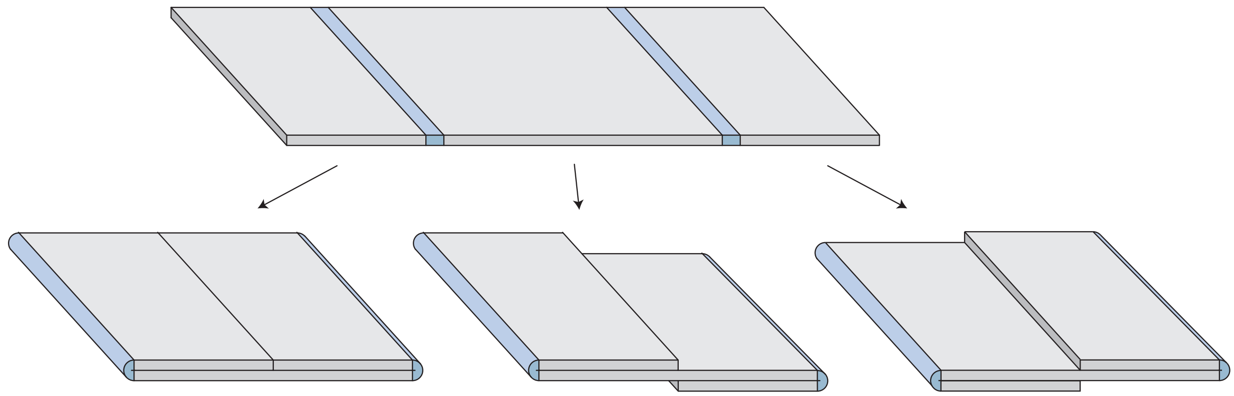

Figure 6.1: Four configuration states of the designed reconfigurable reflectarray. Grey panels are assumed to be rigid, while the blue sections denote compliant surrogate hinges. In each configuration, different panels are exposed, creating an entirely different antenna performance.

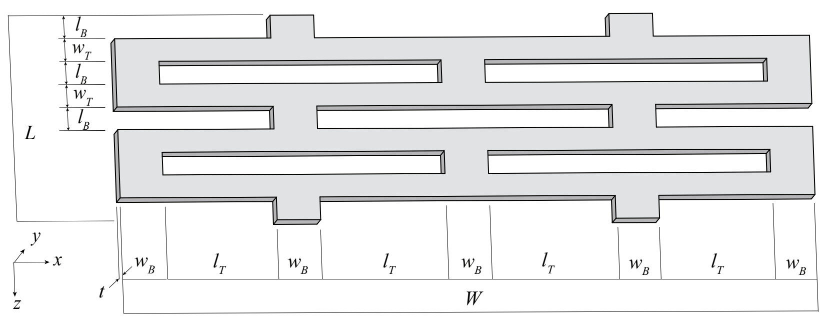

Figure 6.2: Dimensions of a LET array. This diagram shows four LET joints in series and in parallel, making a 2 x 2 LET array.

surrogate hinges on either side of a solid PCB panel enables the spatial reconfiguration of the RA into the four folding states shown in Figure 6.1.

The exact dimensions of the LET joint hinge are dependent on the thickness of the panel, desired total angle of panel rotation, desired stiffness, and the mechanical properties of the material. For this work, 0.787 mm thick Rogers 5880 RA high frequency laminate with 0.5 oz copper cladding was used in this foldable RA. It is important to note that this design could be adjusted for different materials and thicknesses to achieve various ranges of motion and stiffnesses.

A LET array is comprised of several individual LET joints placed in series and in parallel, attached to rigid panels on either side. A detailed diagram of the LET joint dimensions used in this design is shown in Figure 6.2.

The rotational stiffness of a LET array in the out-of-plane (x-direction) is

$$k_{eq,x} = \frac{Pk_T k_B}{S(k_B + \frac{2P+1}{(P+1)}k_T) + k_T} \tag{6.1}$$

where k_T is the stiffness of the torsional sections, k_B is the stiffness of the bending sections, and where P and S are the amount of LETs in parallel and series, respectively [62]. The in-plane rotational stiffness (y-direction) is given by

$$k_{eq,y} = \frac{\delta M_y}{\delta \beta} \tag{6.2}$$

where M_y is the bending moment about the y-axis and β is the rotational displacement. Unlike the stiffness about the x-axis (Eqn. 6.1), the stiffness about the y-axis is nonlinear and requires an iterative solution. Ref. [62] describes the algorithm to determine the stiffness about the y-axis. DeFigueiredo [155] showed that the maximum Von Mises equivalent stress in an S-series LET array is

$$\sigma_{max} = \frac{2k_T k_B \theta}{S(k_T + 2k_B)} \sqrt{\frac{9}{w_B^2 t^4} + \frac{3}{4Q^2}} \tag{6.3}$$

where θ is the angle of rotation of the whole array in radians, t is the thickness of the array, and Q is a geometry dependent parameter defined as

$$Q = \frac{w_T^2 t^2}{3w_T + 1.8t} \tag{6.4}$$

6.2.2 LET Array Design Optimization

An optimization routine was performed to define dimensions for the LET array joint. While the desired motion of the LET joint is an out-of-plane rotation, other undesirable "parasitic" motions can also occur as the joint has 6 degrees of freedom (DOF). Researchers have characterized LET joints according to many of these DOF [20, 62, 155]. The surrogate joint is used to simulate a pin-joint and precise motion of the joint is important. For these reasons, the purpose of the optimization was to maximize the resistance to in-plane rotation (parasitic motion) in comparison to out-of-plane rotation (desired folding) of the array. These motions are shown in Figure 6.3. This was quantified by using the ratio of the stiffnesses (k_y/k_x) as defined in [62].

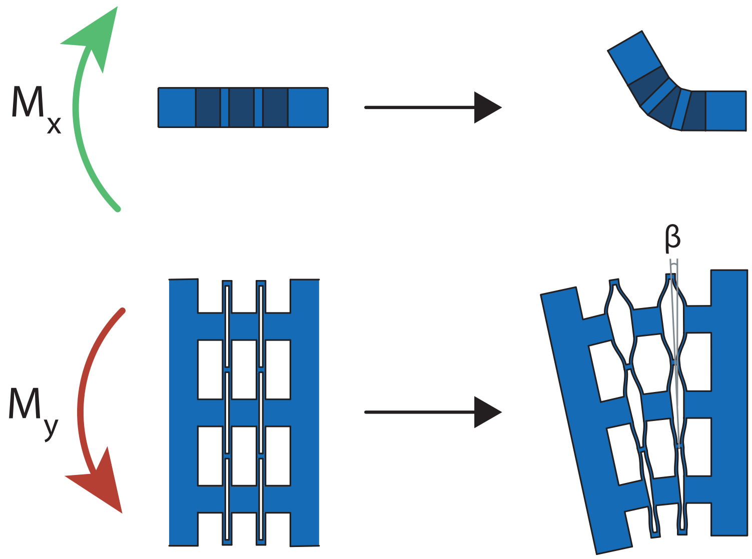

Figure 6.3: Two modes of motion for a LET array: (a) the desired folding panel motion (applied moment around x-axis), and (b) the undesired in-plane parasitic motion (applied moment around y-axis).

The optimization was constrained to design a LET array that would not fail due to stresses when folded as defined in [155]. Other constraints imposed were that the width, W, of the LET array had to be equal to the width of the panels, w_{array}, and that the LET array length, L, needed to be less than or equal to a specified length, l, see Figure 6.2. Concisely,the objective of the optimization was to

$$
\begin{aligned}
Minimize: &\; -\frac{k_y}{k_x} \\
with\ respect\ to: &\; w_t, l_t, w_b, l_b, P, S \\
subject\ to: &\; \sigma_{maxvonmises} \leq \frac{\sigma_T}{n} \\
&\; L \leq l \\
&\; W = w_{array} \\
&\; P, S \in \mathbb{Z}
\end{aligned}
\tag{6.5}
$$

Lower bounds were chosen based on the smallest dimensions that could be manufactured without greatly increasing the expense of manufacturing. Upper bounds were chosen based on the upper limits of the space (length and width) that the LET array was required to fit in. A constrained optimization algorithm using the 'fmincon' function in MATLAB was initially run. This algorithm was used because of the need for constraints. Code from [62] was modified and used as the objective function. Additionally, because the parallel and series values (P and S respectively) determined in the optimization need to be integers, the initial optimization was refined using a branch and bound approach until satisfactory results were achieved. The optimized dimensions of the LET array are shown in Table 6.1. The resulting parameters of the surrogate fold are presented in Table 6.2.

6.2.3 Finite Element Analysis (FEA)

Using the defined dimensions from the optimization results, an FEA analysis was performed on the joint using ANSYS Workbench. To expedite the FEA calculations, and for simplicity, a single parallel LET joint of the array was analyzed. Since parallel LET joints undergo the same angular displacement, stresses and deflections are the same across the entire joint due to symmetry.

A fixed constraint was placed on the face of one connecting bending segment, and a ramped remote displacement rotation of 180° was placed on the opposite connecting bending segment face. Stress results are shown in Figure 6.4 and show a maximum Von Mises stress of 22.97 MPa. As expected from torsion theory, the maximum stress is located along the edges of the beams in torsion. The arrows in Figure 6.4 show example locations of where the maximum stress is located.

Table 6.1: Optimized LET joint design for hinge-like motion.

Design Variable	Quantity	Units	Optimized Value
w_t	Width of torsion segment	mm	0.79
l_t	Length of torsion segment	mm	26.83
w_b	Width of bending segment	mm	3.79
l_b	Length of bending segment	mm	0.79
P	Number of parallel elements	#	3
S	Number of series elements	#	2

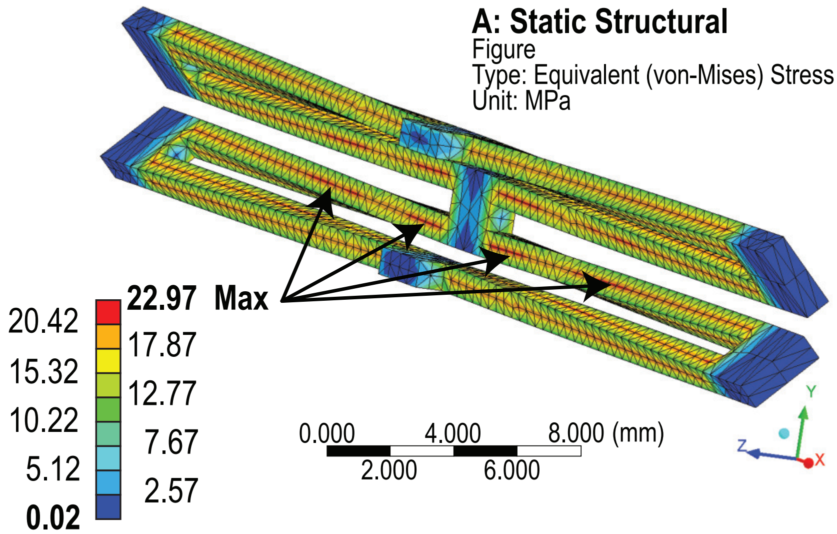

Figure 6.4: Maximum stresses exhibited in the optimized LET joint under a full 180° deflection

In addition, a 180° angular deformation results in a panel displacement of 4.591 mm along the y-axis.

6.2.4 Material Properties

Material properties were obtained from Rogers' Corporation [156] and are presented in Table 6.3. These properties were provided for the x- and z-directions. However, since the equations presented in [62] and [155] are for isotropic materials, the worst-case directional properties (E_x, ν_{xz}, σ_{Tx}) were used. While this introduces some error, a safety factor of 1.2 was added to the optimization stress constraints to account for the possible error

Table 6.2: Resulting surrogate fold parameters for optimized LET design.

Parameter	Quantity	Units	Optimized Value
$k_{eq,x}$	Out-of-plane rotational stiffness	N-mm	1.1
$k_{eq,y}$	In-plane rotational stiffness	N-mm	236.7
$\frac{k_{eq,x}}{k_{eq,y}}$	Stiffness ratio	-	215.2
M_x	Moment to actuate 180°	N-mm	3.6
σ_{max}	Maximum stress	MPa	22.92

6.2.5 Discussion of Results

Analytical and FEA analyses show that the individual elements of the LET array will not exceed the ultimate stress of the Rogers 5880 material when deformed 180° with a pure moment in either direction. Similarly, the fold can also be cycled many times without failure. The actuating moment was solved to be approximately 3.6 N-mm, which is well within the range of standard motor actuators.

Integrating the LET joint into the RA design provides many benefits. First, the surrogate hinge allows the mechanical rotation of the panels ±180° thereby enabling mechanical reconfigurability of the RA. Furthermore, all components of this folding RA design are manufactured from a single planar PCB material. This monolithic design can be made using planar fabrication processes such as micro-milling, stamping, or laser cutting. This is attractive for on-site fabrication in space applications. In addition, since the RA is made from a single planar piece of material, part count and assembly times are greatly reduced. The lower part count also decreases the weight and cost of the RA while the simple manufacturing and little assembly time reduce its production cost. Moreover, since there is no contact between components in the joint, there is no need for lubrication or maintenance considering that this compliant system can be designed to never fatigue.

As mentioned above, the dimensions of the LET array depend on the thickness and stiffness of the panel material. As the thickness or stiffness of the material increases, the LET array will become longer and/or wider, taking up more of the array's usable area. In addition, the resulting moment from the deformation in the LET array may deform the RA enough to affect RA performance. In some configurations with different materials, stress relaxation may become a problem.

Table 6.3: Material properties of Rogers 5880 [156]

Parameter	Quantity	Units	Value
E_x	Out-of-plane rotational stiffness	MPa	2482
E_z	Modulus of elasticity in z-direction	MPa	2206
ν_{xz}	Poisson's ratio in x-direction with applied force in z-direction	-	0.48
ν_{zx}	Poisson's ratio in z-direction with applied force in x-direction	-	0.44
σ_{Tx}	Tensile strength in x-direction	MPa	27.5
σ_{Tz}	Tensile strength in z-direction	MPa	26.2

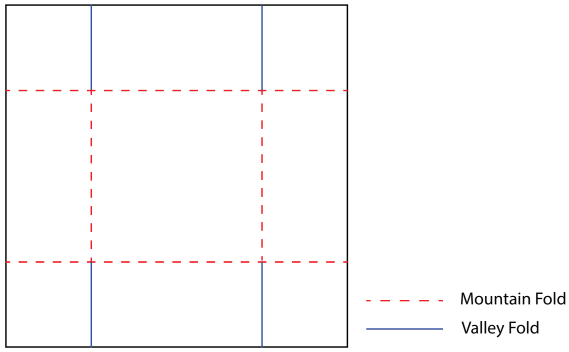

Figure 6.5: Folding pattern for the straight major square twist pattern used in this work. Solid blue lines represent mountain folds, and dotted red lines represent valley folds.

Figure 6.6: Three fold state for paper straight-major square twist.

However, work done by Obaid et al. has showed that the fibers in a composite material may slow the process of stress relaxation [157].

6.3 Deployable Reflectarray Based on the Straight-Major Square Twist Origami Pattern

The high gain RA was mounted onto an origami-inspired folding structure, made from a straight-major square-twist pattern [111]. The fold pattern of a straight-major square-twist is shown in Figure 6.5. This structure was designed to add stiffness to the RA structure, accommodate for material thickness, and enable the RA to fold in a way that exposes three different sets of RA panels. The thickness of the pattern shown also provides built-in stops that limit the motion and keep the panels parallel to each other.

This origami-inspired structure allows for the potential of multiple apertures. When not in use, the structure can be folded and stowed, and when in use, the array can be unfolded into two other configurations. Figure 6.6 shows the three different states to which it folds.

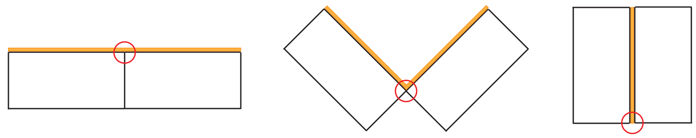

Figure 6.7: Diagram showing how a membrane hinge is applied to a thick-folded origami pattern.

6.3.1 Hinge Design

Each crease in the pattern is created using a membrane hinge [9], as illustrated in Figure 6.7. The membrane used in this design is Kapton® (polyimide), which is a commonly used flexible material for space applications [158, 159]. Because Kapton® is a thermoplastic, it has the potential to be heat set in a desired configuration. This would allow the hinges to be heat set in their deployed configuration. As the hinge is deflected to the closed configuration, strain energy will be stored in the hinges. This strain energy can then be used to deploy the structure. This principle has been shown with polyethylene terephthalate (PET) [160] and parylene in other applications [161]. Repeated deflection loading data for folded Kapton® bellows were reported in [5]. The data shows that Kapton® has a repeated load life exceeding 100,000 cycles and exceeding 30,000 cycles after thermal cycling.

6.3.2 Pattern and Thickness Accommodation

The straight-major square-twist pattern is designed to be both rigid foldable and flat foldable, while also accommodating for the thickness of the material. This pattern utilizes both the split vertex thickness accommodation technique [32, 111], and the hinge shift technique. A diagram of where each thickness accommodation technique was used is shown in Figure 6.8. Chamfers are also used to avoid material interference in the stowed state. For the purposes of concept demonstration, a thickness of 1 cm was arbitrarily chosen for diagrams and prototypes, however, the pattern can be adjusted to accommodate any material thickness for specific applications.

This pattern allows for a footprint increase from stowed to deployed configuration of more than 400% for a 1.0 cm panel thickness, as shown in Figure 6.9(a). This pattern also exhibits a volume packing efficiency of 92%, and would increase as panel thickness is decreased. Packing efficiency was determined as a ratio between the volume of the fully folded state and the volume of the smallest bounding cuboid of that fully folded state, as shown in Figure 6.9(b).

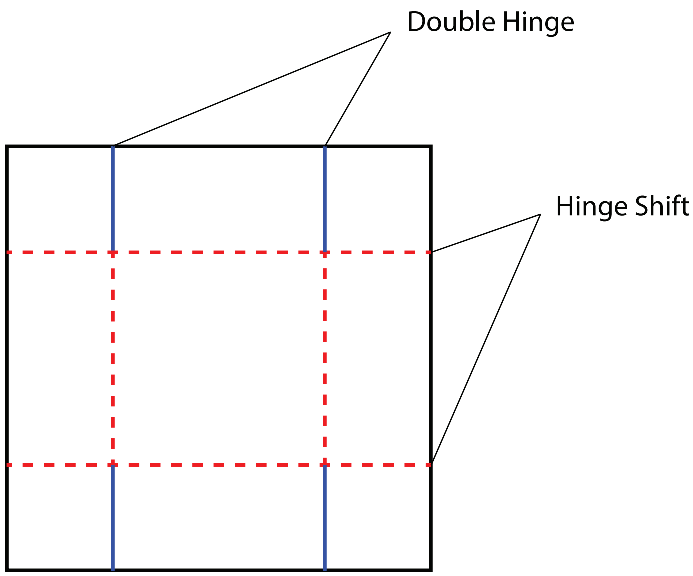

Figure 6.8: Thickness accommodation techniques used in the thickened straight major square twist.

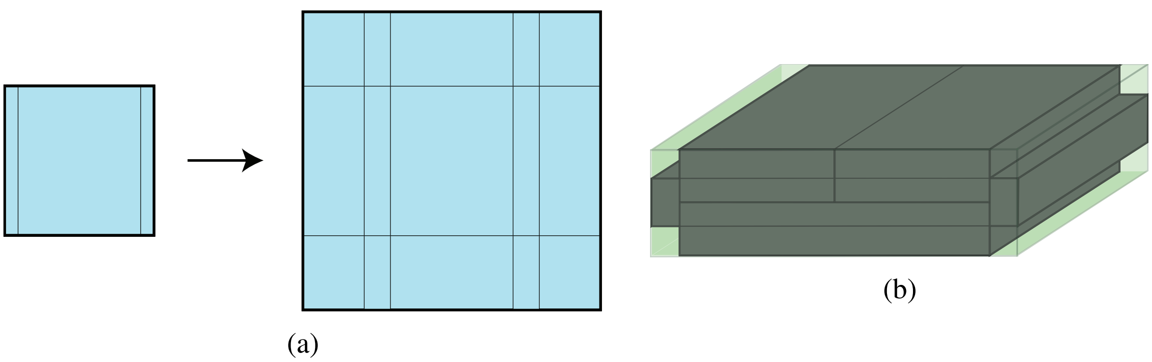

Figure 6.9: (a) illustrates the 400% increase in footprint/aperture for the straight major square twist. The folded structure and its bounding cuboid is shown in (b).

6.3.3 Prototype and Discussion

A demonstration prototype was made using 3D printed PLA structures on which the RA panels were attached. Panels were made to have a 1.0 cm thickness. Individual panels were then attached using 0.127 mm (0.005 inch) thick Kapton® adhesive, which acts as the hinge for the panels to rotate about. Figure6.10 shows this prototype in the three states (stowed, partially deployed, and fully deployed).

While the initial prototype was built using 3D printed PLA structures, the final design will incorporate a structure made of a carbon-fiber reinforced or fiberglass composite material.

Figure 6.10: Three fold state for thickness accommodated straight-major square twist.

Composites are used in space applications because they are lightweight and stiff. The RA panels themselves could also be used alone without the additional composite structure. However, the RA panels are not stiff enough alone and would therefore need additional stiffeners to maintain a flat and parallel orientation.

As mentioned above, the thickness of the structure provides a build-in stop that limits the motion to where the panels remain parallel in each of the three states. However, as the thickness of the structure is reduced, these built-in stops are eliminated and other forms of stiffening need to be incorporated in order to produce an array with the required flatness. Some possibilities include using deployable hard stops [162, 163], using bistable vertices [164, 165], or stored strain energy in the hinge material. In addition to providing stiffening, using deployable hard stops or stored strain energy can allow the structure to be self-deployable [166–168].

While the concept and prototype shown here illustrates a single RA design being stowed and deployed, this structure could be used to expose multiple RA apertures. For each of the configurations shown in Figure 6.10, RA panels could be specifically designed for and placed onto the exposed panels. This would allow a deployable, physically reconfigurable RA design, with three distinct RA apertures and behaviors.

6.4 Physically Reconfigurable Reflectarray Based on the Augmented Square Twist Pattern

6.4.1 Fold Pattern

The square twist is an origami fold pattern that incorporates four degree-4 vertices to enable motion between stowed and fully deployed states. While many angles can be chosen for the square twist pattern, a central square angle, θ, of 45-degrees maximizes the ratio between the deployed and stowed apertures. In addition to changing the angles, different variations of the square twist

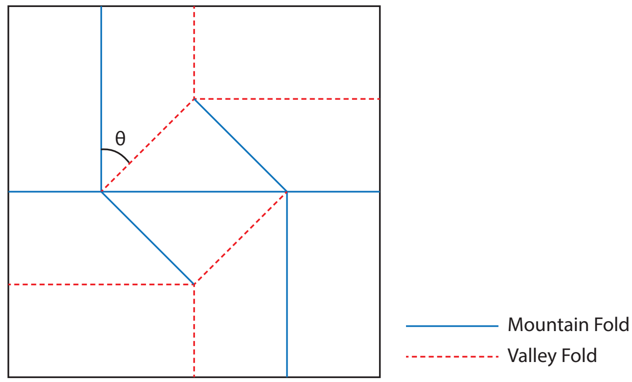

Figure 6.11: Folding pattern for the augmented square twist pattern used in this work. Solid blue lines represent mountain folds, and dotted red lines represent valley folds. The central square angle is defined by θ.

mechanism can be made by using different combinations of crease assignments (mountain/valley). Feng et al. showed which variations of the square twist are rigid foldable – that is they do not require deflection of the pattern panels [169]. They also showed that a non-rigid foldable square twist can be adjusted to become rigid foldable by adding a crease in the middle of the pattern. This adjusted square twist pattern is referred to as the "augmented square twist" pattern [169, 170].

Each of these variations of the square twist mechanism expose sections of different panels when in the fully stowed state. The stowed state of the augmented square twist pattern exposes two coplanar panels, while other variations expose sections of four different parallel panels not on the same plane. In addition, the augmented square twist maintains coplanar panels at the deployed state. For this reason, the augmented square twist was chosen for our proposed RA. Figure 6.11 illustrates the folding pattern for the augmented square twist used in this work. This pattern defines ten individual panels with hinges at the folds allowing rotations necessary for folding.

6.4.2 Thickness Accommodation

With any variation of the square twist, adjustments must be made to accommodate for material thickness. Traditional origami implements folds into paper, and thickness of the folded material can generally be ignored. However, when using engineering materials, such as fiber reinforced panels, thickness cannot be ignored, and adjustments must be made to the design to

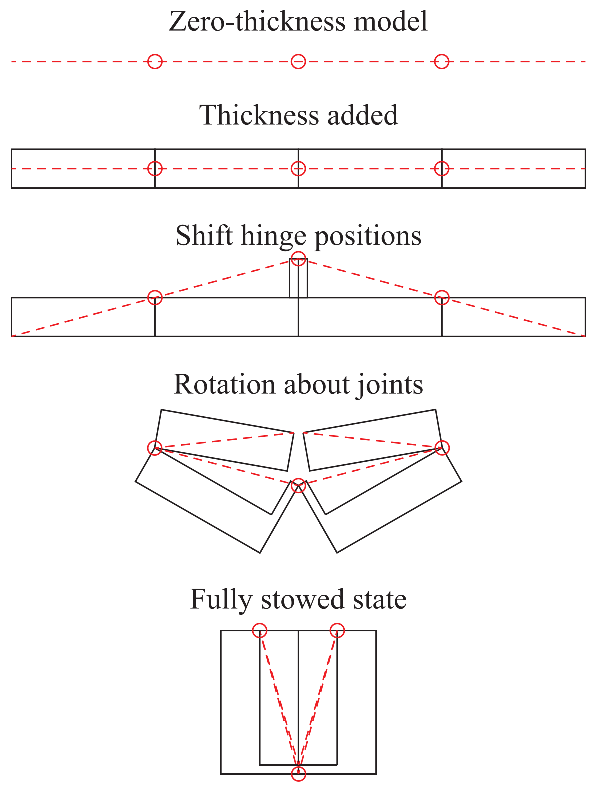

Figure 6.12: Diagram showing the implementation of the hinge shift technique in the augmented square twist. While this diagram shows four planar linkages, they represent spherical linkages for each vertex in the augmented square twist.

accommodate thickness while maintaining mobility. Lang et al. showed a number of thickness accommodating techniques that can be used to adjust designs for an arbitrary thickness [35].

For this work, the hinge-shift technique was used to accommodate for thickness while maintaining rigid foldability, full range of motion, and flat foldability. A diagram of how the hinge shift was implemented into the augmented square twist is shown in Figure 6.12. A proof-of-concept prototype of the folding mechanism was made from 3-D printed PLA with panels connected by adhesive spinnaker tape to create hinges. The panel thickness was arbitrarily chosen to be 3 mm, and the overall pattern width and height to be 150 mm. As mentioned above, thickness was accommodated through the hinge shift technique. Figure 4 shows the stowed, intermediate and fully deployed states of a paper augmented square twist, and thickness accommodated version with thick rigid panels.

While this prototype's dimensions were chosen arbitrarily, they could be customized to any desired deployed aperture and other panel thicknesses. It is important to note that if the ratio

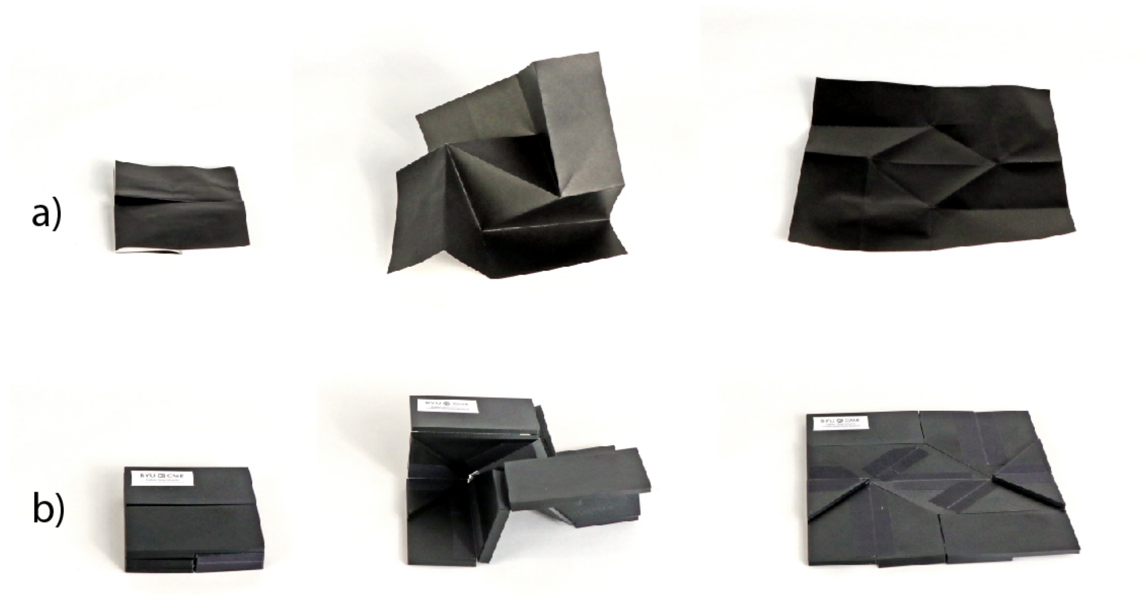

Figure 6.13: Progression of the augmented square twist pattern from fully stowed to fully deployed for both (a) paper and (b) thick rigid panel prototypes.

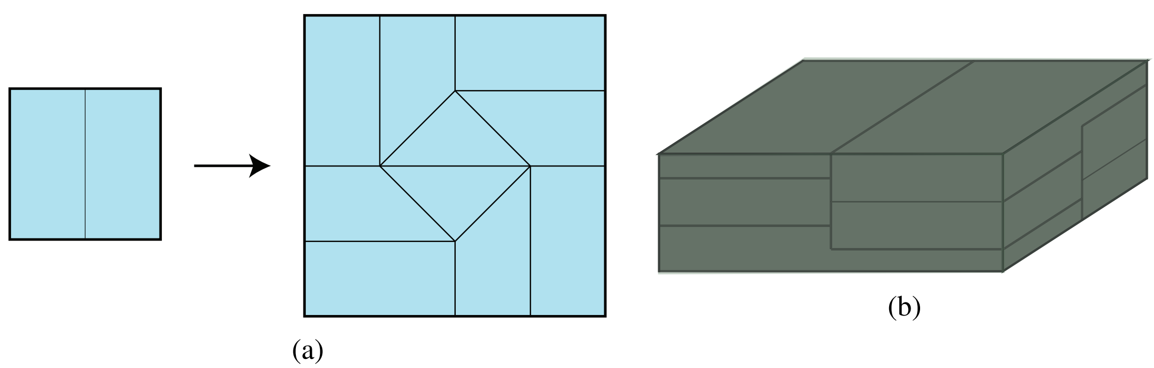

Figure 6.14: (a) illustrates the 400% increase in footprint/aperture for the augmented square twist pattern. The folded structure and its bounding cuboid is shown in (b).

between panel thickness and length becomes too large, another thickness accommodation method may be required.

The augmented square twist fold pattern has a stowed-to-deployed footprint/aperture increase of 400%, as shown in Figure 6.14(a). This pattern also exhibits a volume packing efficiency of 100%. Packing efficiency was determined as a ratio between the volume of the fully folded state and the volume of the smallest bounding cuboid of that fully folded state, as shown in Figure 6.14(b).

Specifically designed RA panels can be modularly incorporated into the folding mechanism. Attaching them to the top face of this mechanism enables the RA to have two mechanical states, stowed and deployed. These two mechanical states expose two different apertures and give the RA two distinct EM behaviors.

CHAPTER 7. CONCLUSION AND FUTURE WORK

7.1 Conclusion

This thesis has presented techniques designers can use when designing deployable systems, with special focus on joint function and utilization. In deployable systems, the selection and arrangement of joint types is key to how the system functions. The kinematics and performance of an array is directly affected by joint performance. While often a single type of joint is used throughout an array, using multiple types of joints within the same array can offer benefits for motion deployability, and stability.

Using compliant joints in deployable arrays give opportunity for parasitic motions to occur. However, motions that are generally undesirable can be utilized to enable motion. In situations where compliant joints are not required to provide a prescribed motion, parasitic motions are not of concern and compliant joints can be used for other benefits such as strain energy storage. This work has provided evidence that utilizing multiple types of joints within a single array can give additional benefits to the system. Benefits may include stored strain energy used for deployment, or stability added to the system through interference.

Folds within an origami array create the constraints that link motion between panels. These constraints can be used to create kinematic benefits, such as creating a 1-DoF system. While many of these fold-constraints are needed to define the motion, this work has shown that many are redundant within origami-based systems. The removal of redundant joints does not effect the motion of the array nor the observed DoF. This work has introduced approaches designers can use to identify redundant constraints in origami patterns, as well as techniques that can be used to remove the redundant constraints. However, the dynamics of the system would be effected.

Current arrays generally utilize joints with pins, barrels, and leafs, using compliant joints provides opportunities

7.2 Future Work

This work has shown that various combinations of redundant joints can be removed from an array while not affecting the system kinematics. However, arrays with various combinations of removed joints would exhibit different dynamic performances. For example, having many single cuts spread evenly throughout the system would likely perform differently than a few longer consecutive cuts across multiple joints. Future work may include analysis and comparison of various combinations of removed joints and their relative performances. Performances of interest may include ease of actuation and stiffnesses against external loads.

Because only a fraction of the total number of joints is needed to define the system kinematics, this work has shown that redundant hinges can be replaced with strain-storing joints. Since these joints can be placed in many combinations of locations, future work could also include analysis of placement of strain-storing joints within an array. Joint placement combinations could be optimized for deployment force, uniform deployment, or stability in the deployed state.

REFERENCES

[1] Yu, H., Guo, Z., and Wang, J., 2018. "A method of calculating the degree of freedom of foldable plate rigid origami with adjacency matrix." *Advances in Mechanical Engineering,* **10**(6), p. 1687814018779696. vii, 18, 21, 22, 23, 26

[2] Howell, L. L., 2001. *Compliant Mechanisms*. John Wiley & Sons. 1, 9, 57

[3] Edmondson, B. J., Bowen, L. A., Grames, C. L., Magleby, S. P., Howell, L. L., and Bateman, T. C., 2013. "Oriceps: Origami-inspired forceps." In *ASME 2013 conference on smart materials, adaptive structures and intelligent systems*, American Society of Mechanical Engineers, p. V001T01A027. 1

[4] Sargent, B., Butler, J., Seymour, K., Bailey, D., Jensen, B., Magleby, S., and Howell, L., 2020. "An origami-based medical support system to mitigate flexible shaft buckling." *Journal of Mechanisms and Robotics,* **12**(4). 1

[5] Butler, J., Morgan, J., Pehrson, N., Tolman, K., Bateman, T., Magleby, S. P., and Howell, L. L., 2016. "Highly compressible origami bellows for harsh environments." In *ASME 2016 International Design Engineering Technical Conferences and Computers and Information in Engineering Conference*, American Society of Mechanical Engineers, p. V05BT07A001. 1, 71

[6] Novelino, L. S., Ze, Q., Wu, S., Paulino, G. H., and Zhao, R., 2020. "Untethered control of functional origami microrobots with distributed actuation." *Proceedings of the National Academy of Sciences,* **117**(39), pp. 24096–24101. 1

[7] Kuribayashi, K., Tsuchiya, K., You, Z., Tomus, D., Umemoto, M., Ito, T., and Sasaki, M., 2006. "Self-deployable origami stent grafts as a biomedical application of ni-rich tini shape memory alloy foil." *Materials Science and Engineering: A,* **419**(1-2), pp. 131–137. 1

[8] Du, Y., Song, C., Xiong, J., and Wu, L., 2019. "Fabrication and mechanical behaviors of carbon fiber reinforced composite foldcore based on curved-crease origami." *Composites Science and Technology,* **174**, pp. 94–105. 1

[9] Zirbel, S. A., Lang, R. J., Thomson, M. W., Sigel, D. A., Walkemeyer, P. E., Trease, B. P., Magleby, S. P., and Howell, L. L., 2013. "Accommodating thickness in origami-based deployable arrays." *Journal of Mechanical Design,* **135**(11), p. 111005. 1, 3, 4, 32, 54, 57, 71

[10] Guang, C., and Yang, Y., 2018. "An approach to designing deployable mechanisms based on rigid modified origami flashers." *Journal of Mechanical Design,* **140**(8). 1

[11] Pehrson, N. A., Ames, D. C., Smith, S. P., Magleby, S. P., and Arya, M., 2020. "Self-deployable, self-stiffening, and retractable origami-based arrays for spacecraft." *AIAA Journal*, pp. 1–8. 1, 4, 41, 42, 55, 59, 60

[12] Shah, S. I. H., Bashir, S., Ashfaq, M., Altaf, A., and Rmili, H., 2021. "Lightweight and low-cost deployable origami antennas-a review." *IEEE Access*. 1, 15

[13] Liu, X., Georgakopoulos, S. V., and Rao, S., 2017. "A design of an origami reconfigurable qha with a foldable reflector [antenna applications corner]." *IEEE Antennas and Propagation Magazine,* **59**(4), pp. 78–105. 1

[14] Kaddour, A.-S., Zekios, C. L., and Georgakapoulos, S. V., 2020. "A reconfigurable origami reflectarray." In *2020 14th European Conference on Antennas and Propagation (EuCAP)*, IEEE, pp. 1–4. 1, 14

[15] Russo, N. E., Zekios, C. L., and Georgakopoulos, S. V., 2019. "A capacity reconfigurable multimode origami mimo antenna." In *2019 IEEE International Symposium on Antennas and Propagation and USNC-URSI Radio Science Meeting*, IEEE, pp. 411–412. 1

[16] Chahat, N., Decrossas, E., and Michael Kobayashi, M., 2020. "Mars cube one." *CubeSat Antenna Design*, pp. 35–89. 1, 15, 54, 57, 58

[17] c Mathew, B., Raikwar, M., Negi, M. S., Singh, H., et al., 2021. "Compliant mechanism and origami usage in aerospace and space application." In *IOP Conference Series: Earth and Environmental Science*, Vol. 775, IOP Publishing, p. 012008. 1, 15

[18] Bhattarai, S., Kim, H., and Oh, H.-U., 2020. "Cubesat's deployable solar panel with viscoelastic multilayered stiffener for launch vibration attenuation." *International Journal of Aerospace Engineering,* **2020**. 1, 15

[19] Bhattarai, S., Go, J.-S., Kim, H., and Oh, H.-U., 2021. "Development of a novel deployable solar panel and mechanism for 6u cubesat of step cube lab-II." *Aerospace,* **8**(3), p. 64. 1, 15

[20] Jacobsen, J. O., Chen, G., Howell, L. L., and Magleby, S. P., 2009. "Lamina emergent torsional (let) joint." *Mechanism and Machine Theory,* **44**(11), pp. 2098–2109. 1, 4, 7, 54, 57, 65

[21] Cannon, J. R., and Howell, L. L., 2005. "A compliant contact-aided revolute joint." *Mechanism and Machine Theory,* **40**(11), pp. 1273–1293. 1, 3, 4, 54, 57

[22] Halverson, P. A., Howell, L. L., and Magleby, S. P., 2010. "Tension-based multi-stable compliant rolling-contact elements." *Mechanism and machine theory,* **45**(2), pp. 147–156. 1, 3, 4, 54, 57

[23] Butler, J., Pehrson, N., and Magleby, S., 2019. "Thick folding through regionally-sandwiched compliant sheets." In *International Design Engineering Technical Conferences and Computers and Information in Engineering Conference*, Vol. 59247, American Society of Mechanical Engineers, p. V05BT07A041. 1, 4, 54, 57

[24] Brown, N. C., Pruett, H. T., Bolanos, D. S., Jackson, C., Beatson, B., Magleby, S. P., and Howell, L. L., 2021. "Origami-inspired systems that improve adult diaper performance to enhance user dignity." *Wearable Technologies,* **In review**. 2

[25] Brown, N. C., Ynchausti, C., Lytle, A., Howell, L. L., and Magleby, S. P., 2021. "Approaches for minimizing joints in single-degree-of-freedom origami-based mechanisms." *Journal of Mechanical Design,* **In review**. 2

[26] Kaddour, A.-S., Velez, C. A., and Georgakopoulos, S. V., 2020. "A deployable and reconfigurable origami reflectarray based on the miura-ori pattern." In *2020 IEEE International Symposium on Antennas and Propagation and North American Radio Science Meeting*, IEEE, pp. 91–92. 2, 14, 41, 63

[27] Rubio, A. J., Kaddour, A.-S., Georgakopoulos, S. V., Brown, N., Ynchausti, C., Howell, L., and Magleby, S., 2021. "An origami-inspired foldable reflectarray on a straight-major square-twist pattern." In *2021 IEEE 21st Annual Wireless and Microwave Technology Conference (WAMICON)*, IEEE, pp. 1–4. 2, 40, 63

[28] Rubio, A. J., Kaddour, A.-S., Brown, N. C., Howell, L. L., Magleby, S., and Georgakopoulos, S. V., 2021. "A physically reconfigurable origami reflectarray based on the augmented square twist." In *2021 IEEE Texas Symposium on Wireless and Microwave Circuits and Systems (WMCS)*, IEEE. 2, 40, 63

[29] Tachi, T., 2011. "Rigid-foldable thick origami." *Origami,* **5**, pp. 253–264. 3, 46

[30] Edmondson, B. J., Lang, R. J., Magleby, S. P., and Howell, L. L., 2014. "An offset panel technique for thick rigidily foldable origami." In *International Design Engineering Technical Conferences and Computers and Information in Engineering Conference*, Vol. 46377, American Society of Mechanical Engineers, p. V05BT08A054. 3

[31] Edmondson, B. J., Lang, R. J., Morgan, M. R., Magleby, S. P., and Howell, L. L., 2015. "Thick rigidly foldable structures realized by an offset panel." *Origami6: I. Mathematics*, p. 149. 3, 32

[32] Ku, J. S., and Demaine, E. D., 2016. "Folding flat crease patterns with thick materials." *Journal of Mechanisms and Robotics,* **8**(3). 3, 71

[33] Lang, R. J., Nelson, T., Magleby, S., and Howell, L., 2017. "Thick rigidly foldable origami mechanisms based on synchronized offset rolling contact elements." *Journal of Mechanisms and Robotics,* **9**(2). 3, 4, 54, 57

[34] Pehrson, N. A., Magleby, S. P., Lang, R. J., and Howell, L. L., 2016. "Introduction of monolithic origami with thick-sheet materials." In *Proceedings of IASS Annual Symposia*, Vol. 2016, International Association for Shell and Spatial Structures (IASS), pp. 1–10. 3

[35] Lang, R. J., Tolman, K. A., Crampton, E. B., Magleby, S. P., and Howell, L. L., 2018. "A review of thickness-accommodation techniques in origami-inspired engineering." *Applied Mechanics Reviews,* **70**(1). 3, 46, 50, 75

[36] Delimont, I. L., Magleby, S. P., and Howell, L. L., 2015. "Evaluating compliant hinge geometries for origami-inspired mechanisms." *Journal of Mechanisms and Robotics,* **7**(1). 4, 7, 54

[37] Wilding, S. E., Howell, L. L., and Magleby, S. P., 2012. "Introduction of planar compliant joints designed for combined bending and axial loading conditions in lamina emergent mechanisms." *Mechanism and Machine Theory,* **56**, pp. 1–15. 4, 7, 54, 57

[38] Chen, G., Magleby, S. P., and Howell, L. L., 2018. "Membrane-enhanced lamina emergent torsional joints for surrogate folds." *Journal of Mechanical Design,* **140**(6). 4, 7, 54, 57, 58

[39] Xie, Z., Qiu, L., and Yang, D., 2017. "Design and analysis of outside-deployed lamina emergent joint (od-lej)." *Mechanism and Machine Theory,* **114**, pp. 111–124. 4, 7, 54, 57

[40] Xie, Z., Qiu, L., and Yang, D., 2018. "Design and analysis of a variable stiffness inside-deployed lamina emergent joint." *Mechanism and Machine Theory,* **120**, pp. 166–177. 4, 7, 54

[41] Xie, Z., Qiu, L., and Yang, D., 2018. "Using the parts used to be removed to improve compliant joint's performance." In *International Design Engineering Technical Conferences and Computers and Information in Engineering Conference*, Vol. 51807, American Society of Mechanical Engineers, p. V05AT07A006. 7

[42] Ku, J. S., 2017. "Folding thick materials using axially varying volume trimming." In *International Design Engineering Technical Conferences and Computers and Information in Engineering Conference*, Vol. 58189, American Society of Mechanical Engineers, p. V05BT08A044. 4, 54, 57

[43] Lang, R. J., Brown, N., Ignaut, B., Magleby, S., and Howell, L., 2020. "Rigidly foldable thick origami using designed-offset linkages." *Journal of Mechanisms and Robotics,* **12**(2). 4, 54, 57

[44] Davis, N. J., and Wyman, J. F., 2020. "Managing urinary incontinence." *AJN The American Journal of Nursing,* **120**(2), pp. 55–60. 6

[45] Lekan-Rutledge, D., Doughty, D., Moore, K. N., and Wooldridge, L., 2003. "Promoting social continence: products and devices in the management of urinary incontinence." *Urologic Nursing,* **23**(6), pp. 416–429. 6

[46] DeMarinis, M., Kaschak, T. R., and Newman, D. K., 2018. "Absorbent products for incontinence." In *Clinical Application of Urologic Catheters, Devices and Products*. Springer, pp. 149–172. 6

[47] Abrams, P., Cardozo, L., Khoury, S., and Wein, A. J., 2013. *Incontinence: 2013*. International Consultation on Urological Diseases. 6

[48] Haylen, B. T., De Ridder, D., Freeman, R. M., Swift, S. E., Berghmans, B., Lee, J., Monga, A., Petri, E., Rizk, D. E., Sand, P. K., et al., 2010. "An international urogynecological association (iuga)/international continence society (ics) joint report on the terminology for

female pelvic floor dysfunction." *Neurourology and Urodynamics: Official Journal of the International Continence Society,* **29**(1), pp. 4–20. 6

[49] Johannesson, M., O'CONOR, R., Kobelt-Nguyen, G., and Mattiasson, A., 1997. "Willingness to pay for reduced incontinence symptoms." *British Journal of Urology,* **80**(4), pp. 557–562. 6

[50] Gyhagen, M., Åkervall, S., Molin, M., and Milsom, I., 2019. "The effect of childbirth on urinary incontinence: a matched cohort study in women aged 40–64 years." *American Journal of Obstetrics and Gynecology,* **221**(4), pp. 322–e1. 6

[51] Constable, L., Cotterill, N., Cooper, D., Glazener, C., Drake, M. J., Forrest, M., Harding, C., Kilonzo, M., MacLennan, G., McCormack, K., et al., 2018. "Male synthetic sling versus artificial urinary sphincter trial for men with urodynamic stress incontinence after prostate surgery (master): study protocol for a randomised controlled trial." *Trials,* **19**(1), pp. 1–17. 6

[52] Nitti, V. W., 2001. "The prevalence of urinary incontinence." *Reviews in Urology,* **3**(Suppl 1), p. S2. 6

[53] Shamliyan, T. A., Wyman, J. F., Ping, R., Wilt, T. J., and Kane, R. L., 2009. "Male urinary incontinence: prevalence, risk factors, and preventive interventions." *Reviews in Urology,* **11**(3), p. 145. 6

[54] Tienza, A., Robles, J. E., Hevia, M., Algarra, R., Diez-Caballero, F., and Pascual, J. I., 2018. "Prevalence analysis of urinary incontinence after radical prostatectomy and influential preoperative factors in a single institution." *The Aging Male,* **21**(1), pp. 24–30. 6

[55] Southall, K., Tuazon, J. R., Djokhdem, A. H., van den Heuvel, E. A., Wittich, W., and Jutai, J. W., 2017. "Assessing the stigma content of urinary incontinence intervention outcome measures." *Journal of Rehabilitation and Assistive Technologies Engineering,* **4**, p. 2055668317738943. 6

[56] Perera, J., Kirthinanda, D. S., Wijeratne, S., and Wickramarachchi, T. K., 2014. "Descriptive cross sectional study on prevalence, perceptions, predisposing factors and health seeking behaviour of women with stress urinary incontinence." *BMC women's health,* **14**(1), pp. 1–7. 6

[57] Siddiqui, N. Y., Levin, P. J., Phadtare, A., Pietrobon, R., and Ammarell, N., 2014. "Perceptions about female urinary incontinence: a systematic review." *International Urogynecology Journal,* **25**(7), pp. 863–871. 6

[58] Devendorf, A. R., Bradley, S. E., Barks, L., Klanchar, A., Orozco, T., and Cowan, L., 2020. "Stigma among veterans with urinary and fecal incontinence." *Stigma and Health*. 6

[59] Milsom, I., Altman, D., Cartwright, R., Lapitan, M., Nelson, R., Sillén, U., and Tikkinen, K., 2013. "Epidemiology of urinary incontinence (ui) and other lower urinary tract symptoms (luts), pelvic organ prolapse (pop) and anal incontinence (ai)." In *Incontinence: 5th International Consultation on Incontinence, Paris, February 2012*. ICUD-EAU, pp. 15–107. 6

[60] Davis, J., 2015. An introduction to adult diapers - their selection and wear. 6

[61] Qiu, L., Yu, Y., and Liu, Y., 2021. "Design and analysis of lamina emergent joint (lej) based on origami technology and mortise-tenon structure." *Mechanism and Machine Theory,* **160**, p. 104298. 7

[62] Pehrson, N. A., Bilancia, P., Magleby, S., and Howell, L., 2020. "Load–displacement characterization in three degrees-of-freedom for general lamina emergent torsion arrays." *Journal of Mechanical Design,* **142**(9). 7, 65, 67, 68

[63] Hamza, M., Zekios, C. L., and Georgakopoulos, S. V., 2019. "A thick origami four-patch array." In *2019 IEEE International Symposium on Antennas and Propagation and USNC-URSI Radio Science Meeting*, IEEE, pp. 1141–1142. 7

[64] Hamza, M., Zekios, C. L., and Georgakopoulos, S. V., 2020. "A thick origami reconfigurable and packable patch array with enhanced beam steering." *IEEE Transactions on Antennas and Propagation,* **68**(5), pp. 3653–3663. 7

[65] Hwang, M., Kim, G., Kim, S., and Jeong, N. S., 2020. "Origami-inspired radiation pattern and shape reconfigurable dipole array antenna at c-band for cubesat applications." *IEEE Transactions on Antennas and Propagation*. 7

[66] Stratton, E., Howell, L., and Bowden, A., 2010. "Force-displacement model of the flexsure™ spinal implant." In *International Design Engineering Technical Conferences and Computers and Information in Engineering Conference*, Vol. 44106, pp. 37–46. 7

[67] Budynas, R. G., Nisbett, J. K., and Tangchaichit, K., 2005. *Shigley's mechanical engineering design*. McGraw Hill New York. 9

[68] Chen, G.-M., and Howell, L. L., 2018. "Symmetric equations for evaluating maximum torsion stress of rectangular beams in compliant mechanisms." *Chinese Journal of Mechanical Engineering,* **31**(1), pp. 1–7. 9

[69] Timoshenko, S., 1940. Strength of materials part 1. 9

[70] Munawar, H. S., 2020. "Reconfigurable origami antennas: A review of the existing technology and its future prospects." *International Journal of Wireless and Microwave Technologies (IJWMT),* **4**, pp. 34–38. 14

[71] Dufour, L., Datashvili, L. S., Guinot, F., Legay, H., and Goussetis, G., 2021. "Origami deployable reflector antenna for cubesats." In *AIAA Scitech 2021 Forum*, p. 1703. 14

[72] Miguélez-Gómez, N., Parkhurst, J. M., Pepin, K., Moline, N., Leblanc, S., Udrea, B., and Rojas-Nastrucci, E. A., 2020. "Thickness-accommodation in x-band origami-based reflectarray antenna for small satellites applications." In *2020 IEEE International Conference on Wireless for Space and Extreme Environments (WiSEE)*, IEEE, pp. 54–59. 14

[73] Johnson, M., Chen, Y., Hovet, S., Xu, S., Wood, B., Ren, H., Tokuda, J., and Tse, Z. T. H., 2017. "Fabricating biomedical origami: A state-of-the-art review." *International journal of computer assisted radiology and surgery,* **12**(11), pp. 2023–2032. 14

[74] Rodrigues, G. V., and Savi, M. A., 2021. "Reduced-order model description of origami stent built with waterbomb." *Sciences,* **472**(2190), p. 20150846. 14

[75] Velvaluri, P., Soor, A., Plucinsky, P., de Miranda, R. L., James, R. D., and Quandt, E., 2021. "Origami-inspired thin-film shape memory alloy devices." *Scientific reports,* **11**(1), pp. 1–10. 14

[76] Liu, C., Maiolino, P., Yang, Y., and You, Z., 2020. "Hybrid soft-rigid deployable structure inspired by thick-panel origami." In *International Design Engineering Technical Conferences and Computers and Information in Engineering Conference*, Vol. 83990, American Society of Mechanical Engineers, p. V010T10A080. 14

[77] Ma, J., Feng, H., Chen, Y., Hou, D., and You, Z., 2020. "Folding of tubular waterbomb." *Research,* **2020**. 14

[78] Tachi, T., 2010. "Geometric considerations for the design of rigid origami structures." In *Proceedings of the International Association for Shell and Spatial Structures (IASS) Symposium*, Vol. 12, Elsevier Ltd, pp. 458–460. 14, 18

[79] Carvalho, M., and Volakis, J. L., 2021. "Performance of partially deployed spaceborne ultra-wideband miura-ori apertures." *IEEE Open Journal of Antennas and Propagation*. 14

[80] Zhang, Y.-J., Wang, L.-C., Song, W.-L., Chen, M., and Fang, D., 2020. "Hexagon-twist frequency reconfigurable antennas via multi-material printed thermo-responsive origami structures." *Frontiers in Materials,* **7**, p. 417. 14

[81] Hamza, M., Zekios, C. L., and Georgakopoulos, S. V., 2021. "A physically reconfigurable 1× 8 monolithic thick origami array." In *2021 IEEE 21st Annual Wireless and Microwave Technology Conference (WAMICON)*, IEEE, pp. 1–3. 14

[82] Bowen, L. A., Grames, C. L., Magleby, S. P., Howell, L. L., and Lang, R. J., 2013. "A classification of action origami as systems of spherical mechanisms." *Journal of Mechanical Design,* **135**(11). 14, 16, 17

[83] Kaddour, A.-S., Velez, C. A., Hamza, M., Brown, N. C., Ynchausti, C., Magleby, S. P., Howell, L. L., and Georgakopoulos, S. V., 2020. "A foldable and reconfigurable monolithic reflectarray for space applications." *IEEE Access,* **8**, pp. 219355–219366. 15, 41, 42

[84] McCarthy, J. M., and Soh, G. S., 2010. *Geometric Design of Linkages*., Vol. 11 Springer Science & Business Media. 16

[85] Chiang, C.-H., 1988. *Kinematics of Spherical Mechanisms*., Vol. 5 Cambridge University Press Cambridge. 16

[86] Hyatt, L. P., Magleby, S. P., and Howell, L. L., 2020. "Developable mechanisms on right conical surfaces." *Mechanism and Machine Theory,* **149**, p. 103813. 16

[87] Barreto, R. L. P., Morlin, F. V., de Souza, M. B., Carboni, A. P., and Martins, D., 2021. "Multiloop origami inspired spherical mechanisms." *Mechanism and Machine Theory,* **155**, p. 104063. 16, 17

[88] Peng, R., Ma, J., and Chen, Y., 2018. "The effect of mountain-valley folds on the rigid foldability of double corrugated pattern." *Mechanism and Machine Theory,* **128**, pp. 461–474. 16

[89] Lang, R. J., 2017. *Twists, tilings, and tessellations: mathematical methods for geometric origami*. CRC Press. 16, 17, 18

[90] Gogu, G., 2005. "Chebychev–grübler–kutzbach's criterion for mobility calculation of multi-loop mechanisms revisited via theory of linear transformations." *European Journal of Mechanics-A/Solids,* **24**(3), pp. 427–441. 17, 18

[91] Mavroidis, C., and Roth, B., 1995. "New and Revised Overconstrained Mechanisms." *Journal of Mechanical Design,* **117**(1), 03, pp. 75–82. 18, 19, 21

[92] Cui, L., and Dai, J. S., 2011. "Axis constraint analysis and its resultant 6r double-centered overconstrained mechanisms." *Journal of Mechanisms and Robotics,* **3**(3). 18, 19, 21, 23

[93] Dai, J. S., Huang, Z., and Lipkin, H., 2004. "Mobility of Overconstrained Parallel Mechanisms." *Journal of Mechanical Design,* **128**(1), 10, pp. 220–229. 18

[94] Zhang, K., and Dai, J. S., 2014. "A kirigami-inspired 8r linkage and its evolved overconstrained 6r linkages with the rotational symmetry of order two." *Journal of Mechanisms and Robotics,* **6**(2), p. 021007. 18

[95] Shen, X., Xu, L., and Li, Q., 2021. "Motion/force constraint indices of redundantly actuated parallel manipulators with over constraints." *Mechanism and Machine Theory,* **165**, p. 104427. 18

[96] Wei, G., and Dai, J. S., 2014. "Origami-inspired integrated planar-spherical overconstrained mechanisms." *Journal of Mechanical Design,* **136**(5), p. 051003. 19, 21

[97] Chen, Y., and You, Z., 2012. "Spatial overconstrained linkages—the lost jade." In *Explorations in the History of Machines and Mechanisms*. Springer, pp. 535–550. 19, 21, 23

[98] Wojtyra, M., 2005. "Joint reaction forces in multibody systems with redundant constraints." *Multibody System Dynamics,* **14**(1), pp. 23–46. 19

[99] Wojtyra, M., and Fraczek, J., 2013. "Comparison of selected methods of handling redundant constraints in multibody systems simulations." *Journal of Computational and Nonlinear Dynamics,* **8**(2). 19

[100] Tachi, T., 2009. "Generalization of rigid-foldable quadrilateral-mesh origami." *Journal of the International Association for Shell and Spatial Structures,* **50**(3), pp. 173–179. 20

[101] Nijenhuis, M., Meijaard, J., and Brouwer, D., 2020. "Misalignments in an overconstrained flexure mechanism: A cross-hinge stiffness investigation." *Precision engineering,* **62**, pp. 181–195. 20

[102] Cammarata, A., 2017. "A novel method to determine position and orientation errors in clearance-affected overconstrained mechanisms." *Mechanism and Machine Theory,* **118**, pp. 247–264. 20

[103] Rameau, J.-F., Serré, P., and Moinet, M., 2019. "Clearance vs. tolerance for mobile overconstrained mechanisms." *Mechanism and Machine Theory,* **136**, pp. 284–306. 20

[104] Yellowhorse, A., and Howell, L. L., 2016. "Creating rigid foldability to enable mobility of origami-inspired mechanisms." *Journal of Mechanisms and Robotics,* **8**(1). 23, 26, 29, 31

[105] Wiener, M. R., 2016. *A foundation for analysis of spherical system linkages inspired by origami and kinematic paper art*. Lehigh University. 23

[106] Cai, J., Deng, X., Xu, Y., and Feng, J., 2014. "Constraint analysis and redundancy of planar closed loop double chain linkages." *Advances in Mechanical Engineering,* **6**, p. 635423. 26

[107] Cai, J., Qian, Z., Jiang, C., Feng, J., and Xu, Y., 2016. "Mobility and kinematic analysis of foldable plate structures based on rigid origami." *Journal of Mechanisms and Robotics,* **8**(6). 26

[108] Lang, R. J., Brown, N., Ignaut, B., Magleby, S., and Howell, L., 2019. "Rigidly foldable thick origami using designed-offset linkages." In *International Design Engineering Technical Conferences and Computers and Information in Engineering Conference*, Vol. 59247, American Society of Mechanical Engineers, p. V05BT07A035. 27

[109] Bolanos, D., Brown, N. C., Ynchausti, C., Pruett, H., Hunter, J., Clark, B., Bateman, T., Howell, L., and Magleby, S., 2021. "Challenges and opportunities of the miura-ori pattern in deployable space arrays." In *International Conference on Reconfigurable Mechanisms and Robots (ReMAR 2021)*, IEEE/IFToMM. 27, 41

[110] Beatini, V., and Korkmaz, K., 2013. "Shapes of miura mesh mechanism with mobility one." *International Journal of Space Structures,* **28**(2), pp. 101–114. 34, 35

[111] Tolman, K. A., Lang, R. J., Magleby, S. P., and Howell, L. L., 2017. "Split-vertex technique for thickness-accommodation in origami-based mechanisms." In *International Design Engineering Technical Conferences and Computers and Information in Engineering Conference*, Vol. 58189, American Society of Mechanical Engineers, p. V05BT08A054. 39, 70, 71

[112] Thomson, M. W., 2000. "The astromesh deployable reflector." In *IUTAM-IASS Symposium on Deployable Structures: Theory and Applications*, Springer, pp. 435–446. 40

[113] Yuan, P., He, B., Zhang, L., Jiang, H., Nie, R., and Ma, X., 2021. "Topology generation and optimization of boundary cable nets for the mesh reflector antenna." *Engineering Structures,* **229**, p. 111630. 40

[114] Meshkovsky, V. Y., Sdobnikov, A., and Kisanov, Y. A., 2021. "An approach to design of large-sized deployable hoop space antenna reflector." In *Journal of Physics: Conference Series*, Vol. 1902, IOP Publishing, p. 012125. 40, 41, 42

[115] Entekhabi, D., Njoku, E. G., O'Neill, P. E., Kellogg, K. H., Crow, W. T., Edelstein, W. N., Entin, J. K., Goodman, S. D., Jackson, T. J., Johnson, J., et al., 2010. "The soil moisture active passive (smap) mission." *Proceedings of the IEEE,* **98**(5), pp. 704–716. 40

[116] Chahat, N., Sauder, J., Hodges, R., Thomson, M., Samii, Y. R., and Peral, E., 2016. "Ka-band high-gain mesh deployable reflector antenna enabling the first radar in a cubesat: Raincube." In *2016 10th European Conference on Antennas and Propagation (EuCAP)*, IEEE, pp. 1–4. 40, 41, 42

[117] Gdoutos, E., Truong, A., Pedivellano, A., Royer, F., and Pellegrino, S., 2020. "Ultralight deployable space structure prototype." In *AIAA Scitech 2020 Forum*, p. 0692. 40, 41

[118] Liu, Z.-Q., Qiu, H., Li, X., and Yang, S.-L., 2017. "Review of large spacecraft deployable membrane antenna structures." *Chinese Journal of Mechanical Engineering,* **30**(6), pp. 1447–1459. 40

[119] Chandra, M., Kumar, S., Chattopadhyaya, S., Chatterjee, S., and Kumar, P., 2021. "A review on developments of deployable membrane-based reflector antennas." *Advances in Space Research*. 40

[120] Arya, M., Sauder, J. F., Hodges, R., and Pellegrino, S., 2019. "Large-area deployable reflectarray antenna for cubesats." In *AIAA Scitech 2019 Forum*, p. 2257. 40

[121] Babuscia, A., Corbin, B., Knapp, M., Jensen-Clem, R., Van de Loo, M., and Seager, S., 2013. "Inflatable antenna for cubesats: Motivation for development and antenna design." *Acta Astronautica,* **91**, pp. 322–332. 40

[122] Babuscia, A., Choi, T., Sauder, J., Chandra, A., and Thangavelautham, J., 2016. "Inflatable antenna for cubesats: Development of the x-band prototype." In *2016 IEEE Aerospace Conference*, IEEE, pp. 1–11. 40

[123] Huang, J., and Feria, A., 1999. "Inflatable microstrip reflectarray antennas at x and ka-band frequencies." In *IEEE Antennas and Propagation Society International Symposium. 1999 Digest. Held in conjunction with: USNC/URSI National Radio Science Meeting (Cat. No. 99CH37010)*, Vol. 3, IEEE, pp. 1670–1673. 40, 41

[124] Babuscia, A., Sauder, J., Chandra, A., Thangavelautham, J., Feruglio, L., and Bienert, N., 2017. "Inflatable antenna for cubesat: A new spherical design for increased x-band gain." In *2017 IEEE Aerospace Conference*, IEEE, pp. 1–10. 40, 41

[125] Huang, H., Cheng, Q., and Zheng, L., 2020. "Structural dynamic improvement for petal-type deployable solid-surface reflector based on numerical parameter study." *Applied Sciences,* **10**(18), p. 6560. 40, 41

[126] Sauder, J. F., Arya, M., Chahat, N., Thiel, E., Dunphy, S., Shi, M., Agnes, G., and Cwik, T., 2019. "Deployment mechanisms for high packing efficiency one-meter reflectarray antenna (omera)." In *AIAA Scitech 2019 Forum*, p. 0755. 40, 41, 42

[127] Hodges, R. E., Chahat, N. E., Hoppe, D. J., and Vacchione, J. D., 2016. "The mars cube one deployable high gain antenna." In *2016 IEEE International Symposium on Antennas and Propagation (APSURSI)*, IEEE, pp. 1533–1534. 40, 41, 42

[128] Baoyan, D., 2020. "Large spaceborne deployable antennas (lsdas)-a comprehensive summary." *Chinese Journal of Electronics,* **29**(1), pp. 1–15. 41

[129] Sun, Z., Yang, D., Duan, B., Kong, L., and Zhang, Y., 2021. "Structural design, dynamic analysis, and verification test of a novel double-ring deployable truss for mesh antennas." *Mechanism and Machine Theory,* **165**, p. 104416. 41, 42

[130] Sun, Z., Zhang, Y., and Yang, D., 2021. "Structural design, analysis, and experimental verification of an h-style deployable mechanism for large space-borne mesh antennas." *Acta Astronautica,* **178**, pp. 481–498. 41, 42

[131] Chahat, N., Sauder, J., and Freebury, G., 2020. "X/ka-band one meter mesh reflector for 12u-class cubesat." *CubeSat Antenna Design*, pp. 163–196. 41, 42

[132] Sauder, J. F., Chahat, N., Hirsch, B., Hodges, R., Rahmat-Samii, Y., Peral, E., and Thomson, M. W., 2017. "From prototype to flight: qualifying a ka-band parabolic deployable antenna (kapda) for cubesats." In *4th AIAA Spacecraft Structures Conference*, p. 0620. 41

[133] Sauder, J., Chahat, N., Thomson, M., Hodges, R., Peral, E., and Rahmat-Samii, Y., 2015. "Ultra-compact ka-band parabolic deployable antenna for radar and interplanetary cubesats.". 41

[134] Chamberlain, M. K., Kiefer, S. H., LaPointe, M., and LaCorte, P., 2021. "On-orbit flight testing of the roll-out solar array." *Acta Astronautica,* **179**, pp. 407–414. 41, 42

[135] Hoang, B., White, S., Spence, B., and Kiefer, S., 2016. "Commercialization of deployable space systems' roll-out solar array (rosa) technology for space systems loral (ssl) solar arrays." In *2016 IEEE Aerospace Conference*, IEEE, pp. 1–12. 41, 42

[136] Spence, B. R., White, S., LaPointe, M., Kiefer, S., LaCorte, P., Banik, J., Chapman, D., and Merrill, J., 2018. "International space station (iss) roll-out solar array (rosa) spaceflight experiment mission and results." In *2018 IEEE 7th World Conference on Photovoltaic Energy Conversion (WCPEC)(A Joint Conference of 45th IEEE PVSC, 28th PVSEC & 34th EU PVSEC)*, IEEE, pp. 3522–3529. 41, 42

[137] Banik, J., Kiefer, S., LaPointe, M., and LaCorte, P., 2018. "On-orbit validation of the roll-out solar array." In *2018 IEEE Aerospace Conference*, IEEE, pp. 1–9. 41, 42

[138] Leclerc, C., Wilson, L. L., Bessa, M. A., and Pellegrino, S., 2017. "Characterization of ultra-thin composite triangular rollable and collapsible booms." In *4th AIAA Spacecraft Structures Conference*, p. 0172. 41

[139] Royer, F., and Pellegrino, S., 2018. "Ultralight ladder-type coilable space structures." In *2018 AIAA Spacecraft Structures Conference*, p. 1200. 41

[140] Lan, X., Liu, L., Pan, C., Li, F., Liu, Z., Hou, G., Sun, J., Dai, W., Wang, L., Yue, H., et al., 2021. "Smart solar array consisting of shape-memory releasing mechanisms and deployable hinges." *AIAA Journal,* **59**(6), pp. 2200–2213. 41, 42

[141] Li, Y., Wei, J., and Dai, L., 2020. "Structural design and dynamic analysis of new ultra-large planar deployable antennas in space with locking systems." *Aerospace Science and Technology,* **106**, p. 106082. 42

[142] Lee, A., and Pellegrino, S., 2021. "Cable-stayed architectures for large deployable spacecraft." In *AIAA Scitech 2021 Forum*, p. 1386. 42

[143] Yellowhorse, A., and Howell, L. L., 2018. "Deployable lenticular stiffeners for origami-inspired mechanisms." *Mechanics Based Design of Structures and Machines,* **46**(5), pp. 634–649. 42, 43, 44, 45, 54

[144] Ynchausti, C., Brown, N., Magleby, S. P., Bowden, A. E., and Howell, L. L. "Deployable Euler spiral connectors." *Journal of Mechanisms and Robotics,* **In Review**. 42, 43, 44

[145] Talbot, A. N., 1901. *The railway transition spiral*. Engineering News Publishing Company. 43

[146] Brustad, T. F., and Dalmo, R., 2020. "Railway transition curves: A review of the state-of-the-art and future research." *Infrastructures,* **5**(5), p. 43. 43

[147] Ling, H., and Shabana, A. A., 2021. "Euler angles and numerical representation of the railroad track geometry." *Acta Mechanica*, pp. 1–19. 43

[148] Pahuja, A., Parihar, M. S., and Kumar, V. D., 2018. "Investigation of euler spiral nanoantenna and its application in absorption enhancement of thin film solar cell." *Optical and Quantum Electronics,* **50**(11), pp. 1–11. 43

[149] Ren, H., and Fujisawa, K., 2021. "Obstacle avoidable g2-continuous trajectory generated with clothoid spline solution." In *2021 6th International Conference on Control and Robotics Engineering (ICCRE)*, IEEE, pp. 23–27. 43

[150] Botros, A., and Smith, S. L., 2021. "Tunable trajectory planner using g3 curves." *arXiv preprint arXiv:2106.03836*. 43

[151] Gonthina, P. S., Kapadia, A. D., Godage, I. S., and Walker, I. D., 2019. "Modeling variable curvature parallel continuum robots using euler curves." In *2019 International Conference on Robotics and Automation (ICRA)*, IEEE, pp. 1679–1685. 43

[152] DeFigueiredo, B., Pehrson, N. A., Tolman, K., Crampton, E., Magleby, S. P., and Howell, L. L., 2019. "Origami-based design of conceal-and-reveal systems." *Journal of Mechanisms and Robotics*. 50

[153] Sicre, J., Givois, D., and Emerit, A., 2005. "Application of "maeva" hinge to myriade microsatellites deployments needs." In *11th European Space Mechanisms and Tribology Symposium/ESMATS*, pp. 21–23. 54

[154] Chahat, N., 2021. *CubeSat Antenna Design*. John Wiley & Sons. 58

[155] De Figueiredo, B. P., 2017. "Developing new classes of thick-origami-based mechanisms: Conceal-and-reveal motion and folding printed circuit boards.". 65, 66, 68

[156] Kuszaj, M., 2020. Private Communication. 68, 69

[157] Obaid, N., Kortschot, M. T., and Sain, M., 2018. "Predicting the stress relaxation behavior of glass-fiber reinforced polypropylene composites." *Composites Science and Technology,* **161**, pp. 85–91. 70

[158] Sigel, D., Trease, B. P., Thomson, M. W., Webb, D. R., Willis, P., and Lisman, P. D., 2014. "Application of origami in the starshade spacecraft blanket design." In *International Design Engineering Technical Conferences and Computers and Information in Engineering Conference*, Vol. 46377, American Society of Mechanical Engineers, p. V05BT08A033. 71

[159] Lamoureux, A., Lee, K., Shlian, M., Forrest, S. R., and Shtein, M., 2015. "Dynamic kirigami structures for integrated solar tracking." *Nature communications,* **6**(1), pp. 1–6. 71

[160] Klett, Y., 2018. "Paleo: Plastically annealed lamina emergent origami." In *International Design Engineering Technical Conferences and Computers and Information in Engineering Conference*, Vol. 51814, American Society of Mechanical Engineers, p. V05BT07A062. 71

[161] Liu, Y., Park, J., Lang, R. J., Emami-Neyestanak, A., Pellegrino, S., Humayun, M. S., and Tai, Y.-C., 2013. "Parylene origami structure for intraocular implantation." In *2013 Transducers & Eurosensors XXVII: The 17th International Conference on Solid-State Sensors, Actuators and Microsystems (TRANSDUCERS & EUROSENSORS XXVII)*, IEEE, pp. 1549–1552. 71

[162] Andrews, D. W., Avila, A., Butler, J., Magleby, S. P., and Howell, L. L., 2019. "Kirigami-based deployable transcrease hard stop models usable in origami patterns." In *International Design Engineering Technical Conferences and Computers and Information in Engineering Conference*, Vol. 59247, American Society of Mechanical Engineers, p. V05BT07A044. 73

[163] Shemenski, P. D., and Trease, B. P., 2018. "Compact directional and frictional hinges for flat folding applications." In *International Design Engineering Technical Conferences and Computers and Information in Engineering Conference*, Vol. 51814, American Society of Mechanical Engineers, p. V05BT07A064. 73

[164] Pehrson, N. A., Magleby, S. P., and Howell, L. L., 2018. "An origami-based thickness-accommodating bistable mechanism in monolithic thick-sheet materials." In *2018 International Conference on Reconfigurable Mechanisms and Robots (ReMAR)*, IEEE, pp. 1–7. 73

[165] Walker, M. G., and Seffen, K. A., 2018. "On the shape of bistable creased strips." *Thin-Walled Structures,* **124**, pp. 538–545. 73

[166] Chen, T., Bilal, O. R., Lang, R., Daraio, C., and Shea, K., 2019. "Autonomous deployment of a solar panel using elastic origami and distributed shape-memory-polymer actuators." *Physical Review Applied,* **11**(6), p. 064069. 73

[167] Pedivellano, A., Gdoutos, E., and Pellegrino, S., 2020. "Sequentially controlled dynamic deployment of ultra-thin shell structures." In *AIAA Scitech 2020 Forum*, p. 0690. 73

[168] Fulton, J., and Schaub, H., 2019. "Non-symmetric behavior of high strain composite tape spring hinges for folding structures." In *AIAA Scitech 2019 Forum*, p. 1747. 73

[169] Feng, H., Peng, R., Zang, S., Ma, J., and Chen, Y., 2020. "Rigid foldability and mountain-valley crease assignments of square-twist origami pattern." *Mechanism and Machine Theory,* **152**, p. 103947. 74

[170] Hull, T. C., and Urbanski, M. T., 2018. "Rigid foldability of the augmented square twist." *arXiv preprint arXiv:1809.04899*. 74